Agricultural Water Management 277 (2023) 108125

Contents lists available at ScienceDirect

Agricultural Water Management

journal homepage: www.elsevier.com/locate/agwat

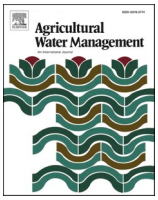

Application of inclusive multiple model for the prediction of saffron water footprint

Zahra Gerkani Nezhad Moshizi [a], Ommolbanin Bazrafshan [a,*], Hadi Ramezani Etedali [b], Yahya Esmaeilpour [a], Brain Collins [c]

[a] Department of Natural Resources Engineering, University of Hormozgan, Bandar Abbas, Iran
[b] Department of Water Sciences and Engineering, Imam Khomeini International University, Qazvin, Iran
[c] College of Science and Engineering, James Cook University, Townsville, QLD 4811, Australia

ARTICLE INFO

Handling Editor - Dr. B.E. Clothier

Keywords:
Water footprint
Saffron
Crop and climate variables
Group method of data handling
Evolutionary algorithms

ABSTRACT

Applying new approaches in the management of water resources is a vital issue, especially in arid and semi-arid regions. The water footprint is a key index in water management. Therefore, it is necessary to predict its changes for future durations. The soft computing model is one of the most widely used models in predicting and estimating agroclimatic variables. The purpose of this study is to predict the green and blue water footprints of saffron product using the soft computing model. In order to select the most effective variables in prediction water footprints, the individual input was eliminated one by one and the effect of each on the residual mean square error (RMSE) was measured. In the first stage, the Group Method of Data Handling (GMDH) and evolutionary algorithms have been applied. In the next stage, the output of individual models was incorporated into the Inclusive Multiple Model (IMM) as the input variables in order to predict the blue and green water footprints of saffron product in three homogenous agroclimatic regions. Finally, the uncertainty of the model caused by the input and parameters was evaluated. The contributions of this research are introducing optimized GMDH and new ensemble models for predicting BWF, and GWF, uncertainty analysis and investigating effective inputs on the GWF and BWF. The results indicated that the most important variables affecting green and blue water footprints are plant transpiration, evapotranspiration, and yield, since removing these variables significantly increased the RMSE (range=11–25). Among the GMDH models, the best performance belonged to NMRA (Naked Mole Ranked Algorithm) due to the fast convergence and high accuracy of the outputs. In this regard, the IMM has a better performance (FSD=0.76, NSE=0.95, MAE) = 8, PBIAS= 8) than the alternatives due to applying the outputs of several individual models and the lowest uncertainty based on the parameters and inputs of the model ($p = 0.98$, $r = 0.08$).

1. Introduction

Population growth, agricultural expansion, industrial development, improvement of living standards, and changes in consumption patterns have caused the water demand to be increased (Siam and Eltahir, 2017; Elbeltagi et al., 2020a; Wang et al., 2021).

The problem of freshwater shortage may intensify in the future due to the increasing demands and decreasing water availability, quantity and quality. This issue will cause problems for food security and environmental sustainability (Rosegrant et al., 2009; Ercin and Hoekstra, 2016).

Almost 85% of global freshwater is consumed in the agricultural sector (Mekonnen and Hoekstra, 2011; Bhat et al., 2017; Elbeltagi et al., 2021). Therefore, water footprint (WF) could be a useful tool for dealing with water security challenges, especially in the agricultural sector (Hoekstra and Hung, 2003; Hoekstra, 2008; Bazrafshan et al., 2019b).

The water footprint (WF) approach was first proposed by Hoekstra in 2003. WF describe the total volume of freshwater that is used directly or indirectly to produce of goods and services (Hoekstra and Hung, 2003; Zhang et al., 2017, 2020; Zhai et al., 2019). WF is a combination of green, blue, and gray water footprints (Jamshidi et al., 2020). The blue WF (BWF) involves the volume of surface and underground water consumption (Hoekstra et al., 2011; Mekonnen and Hoekstra, 2014; Sidhu et al., 2021). The green WF (GWF) denotes the volume of rainwater

* Corresponding author.
E-mail address: O.bazrafshan@hormozgan.ac.ir (O. Bazrafshan).

https://doi.org/10.1016/j.agwat.2022.108125
Received 12 August 2022; Received in revised form 15 December 2022; Accepted 21 December 2022
Available online 2 January 2023

consumed during the growing period of the crop (Wang et al., 2022b; Sidhu et al., 2021; Zhao et al., 2019).

The gray WF is the volume of water required to dilute pollutants tolerably (Hoekstra and Chapagain, 2006; Wang et al., 2022a). WF is a key index in the management of water resources and agriculture. Therefore, the prediction WF is important due to its dependence on various parameters, and its prediction is a complicated issue. In this regard, the soft computing model is one of the appropriate models for predicting and estimating hydrological and agricultural variables.

High accuracy, fast convergence and high flexibility are the characteristics of soft computing models. Previous studies have used different soft computing methods for predicting WF. Elbeltagi et al. (2020b) applied climatic parameters and Artificial Neural Networks (ANNs) model to predict WF. They indicated that the ANN model accurately predicts the blue and green water footprints using the climatic data. Preparing the parameters of the ANN model and determining the number of hidden layers was a research challenge.

Mokhtar et al. (2021) used random forest, decision tree, and incremental regression algorithm to predict the BWF and GWF. They performed their forecast for the future period of 2021–2050 under the conditions of climate change. According to their reports, the BWF and GWF will increase in future periods. Collecting data, preparing climate scenarios and selecting the best model were their research challenges.

Elbeltagi et al. (2021) used climatic parameters such as temperature, wind speed, solar radiation, and vapor pressure to predict WF. They applied four different kernels in the Gaussian model and indicated that the Gaussian algorithm is an appropriate model for estimating WF.

However, various models produce different accuracies. Setting model parameters and collecting required data were the main challenges of their research. The main challenges of the previous studies were determining the input predictors, selecting the best model, and adjusting the parameters. Past researches have focused more on using individual models rather than using an ensemble approach to predict BWF and GWF. Integrated models use optimization algorithms for modeling and then the output of these models is used as the input of the final model. Also, in most past researches, the analysis of uncertainty caused by model parameters and input data has not been considered.

The purpose of the present study is to extract the most effective variables on BWF and GWF, then their prediction based on the optimized ensemble model and finally to analysis the model uncertainty based on the input data and model parameters.

The artificial neural network (ANN) is one of the most important soft computing models. The ANN algorithm is useful for extracting information from imprecise and non-linear data (Adisa et al., 2019). The ANN algorithms have fewer limitations than the conventional approaches (Elbeltagi et al., 2020b). They have various characteristics, including high accuracy, fast computing, and convergence. They also have high analytical power to simulate complex and non-linear problems by applying different mathematical activation functions. (Zhang et al., 1998).

Group Method of Data Handling (GMDH) proposed by Ivakhnenko (1968) is a multivariate analysis approach developed based on the artificial neural network and applied to identify and model complex systems. GMDH model could be used to model complex systems when there is no prior information (Muller and Ivakhnenko, 1996). This method provides more accurate results for low samples and dispersed data than physical models (Ivakhnenko, 1968). Although the GMDH model is a powerful tool, it needs improvements to increase accuracy. The accuracy of the GMDH model directly depends on the estimated parameters. The optimization algorithms are appropriate methods for improving the accuracy of the GMDH model.

The GMDH model is an individual model. Individual models have advantages and disadvantages. However, previous studies showed that ensemble models composed of several individual models have better accuracy than individual models. Therefore, the current research aims to develop the GMDH model using optimization algorithms. Then constructs an ensemble model that involves several optimized GMDH models in order to predict the water footprint of the saffron product.

Saffron is one of the most expensive medicinal plants in the world, that is called red gold (Leone et al., 2018) and is used to treat diseases. This plant is also used as a flavoring, coloring, and preservative in the food industry (Fallahi et al., 2018; Siddique et al., 2020).

Due to its special morphological characteristics, resistance to drought, and its dormant phase that does not require irrigation, saffron needs little water compared to other crops (Kafi et al., 2006; Cardone et al., 2020). These characteristics allow the plant to grow in arid and semi-arid areas (Alizadeh et al., 2009; Agayev et al., 2006).

Saffron is one of the native products of Iran. The importance of saffron can be evaluated from various aspects, such as low water requirement, job creation, preventing the migration of villagers and the livelihood of more than 4,000,000 people (Rastegaripour and Mohammadi, 2018).

Iran with production of 90% of global saffron, has the first rank in terms of cultivated area and production rate in the world (Baghalian et al., 2010; Cardone et al., 2020; Bazrafshan et al., 2019b; Mollafilabi et al., 2020). According to the Ministry of Agricultural Jihad reports published in 2019, the production of saffron in Iran with a cultivated area of 118,372 ha has been 428.19 tons. Khorasan Razavi with 70% of the saffron production and 77% of the saffron cultivation area, has the first rank of saffron production and cultivation area in Iran. After that, Khorasan Jonoobi and Khorasan Shomali provinces have the second and third ranks of saffron production in Iran, respectively (MAJ, 2019).

This study develops the new and optimized GMDH and ensemble models for predicting BWF and GWL. In this regard, we applied the optimization algorithms to improve the GMDH model and estimate its parameters.

Salgotra and Singh (2019) introduced a new optimization algorithm called naked mole rate algorithm (NMRA) to solve optimization problems. The characteristics of this algorithm are high accuracy for solving non-linear optimization, fast convergence, and the ability of training soft computing models. This study uses NMRA optimization algorithm to train GMDH model and estimating parameters. For further investigation, we also applied the GMDH-BA (Bat Algorithm), GMDH-PSO (Particle Swarm Optimization) and GMDH-SA (Shark Smell Algorithm) optimization algorithms to predict the WF. In the second stage, the outputs of the mentioned models are used as the inputs of the IMM (Inclusive Multiple Model) model to predict the WF and evaluate the uncertainty of the model using GLUE. The contributions of current study as follows:

1) Developing a new ensemble method for predicting of BWF and GWF based on optimized GMDH models, 2) this research quantifies the uncertainties of model outputs using a new method.

2. Material and methods

2.1. Case study and data set

Khorasan region in northeastern Iran covering an area 313,335 Km^2, involves three provinces of Khorasan Shomali, Khorasan Razavi and Khorasan Jonoobi, that covers about one-fifth of the Iran land area. These provinces with almost 96% of saffron production (269.12 tons), are the biggest saffron production areas in Iran (Bazrafshan et al., 2019b).

In this research, crop data including cultivation area, saffron production, and the rate of chemical fertilizer consumption in 38 counties are collected from the Ministry of Agricultural Jihad (MAJ, 2021). The meteorological data are taken from the meteorological data source of the Iran (IRIMO, 2021). In this regard, the cultivated area, production, chemical fertilizer consumption, irrigation efficiency, cultivation date and soil type of each region were selected to determine the homogeneous agroclimatic points of saffron production in Khorasan region. In this research, Fuzzy C-Mean (FCM) clustering algorithm was used to

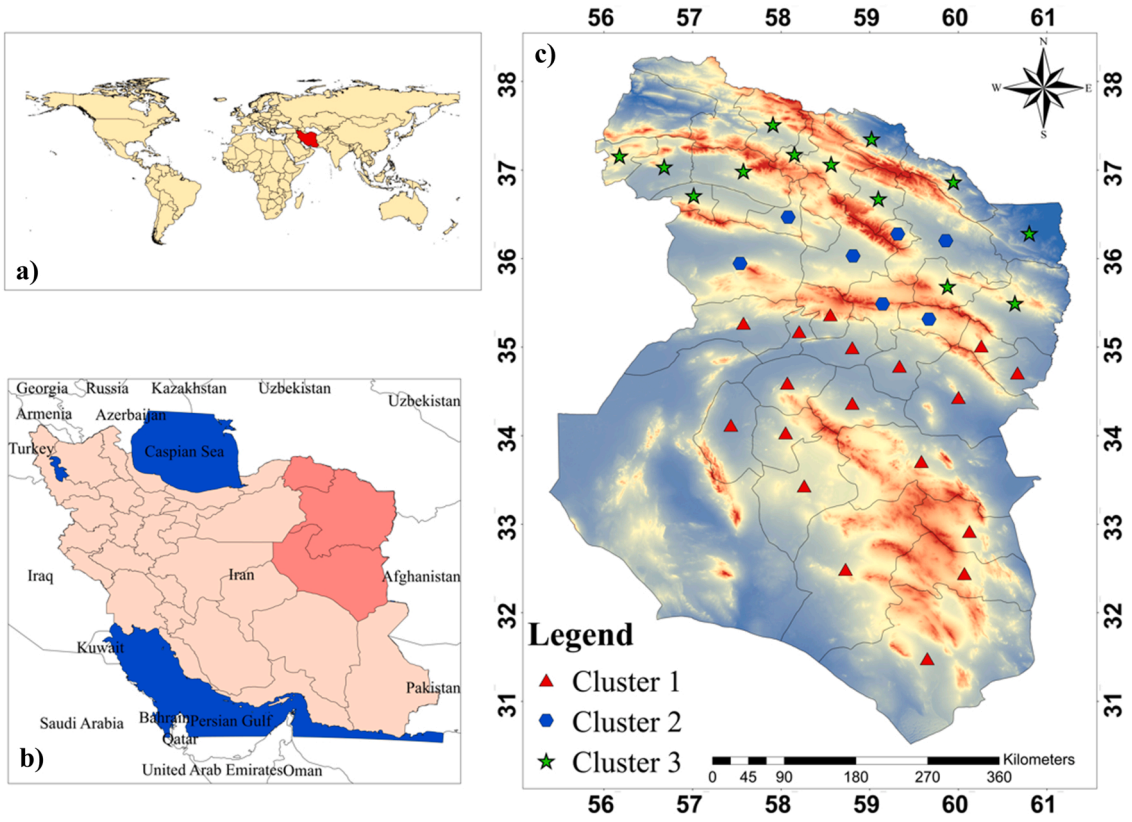

Fig. 1. Homogeneous regions of saffron production in Khorasan province; location of Iran in the world (a); location of Khorasan in Iran (b) and location of clusters in case study (c).

Table 1
Crop information and climatic variables in each cluster at the Khorasan region.

Cluster	I	II	III
Yield (kg/ha)	3.38	3.42	3.67
Fertilizer (kg/ha)	88	84	70
Wind Speed (m/s)	2.54	2.95	2.90
Tmax (°C)	24.48	22.90	21.73
Tmin (°C)	10.70	9.43	8.41
Tmean(°C)	18.40	15.99	15.63
Average Precipitation (mm/day)	135.9	211	232
Relative Humidity (%)	35.5	43.7	49.5
Sunshine Hours (hr)	9	8.6	8.2
Peff (mm)	54.5	62.7	64.9
Etc(mm/day)	839.2	728.8	875.4
IWR (mm)	784.7	666.1	810.7

determine homogeneous points.

2.2. FCM clustering methodology

The purpose of clustering is to divide the observations into several categories in which the observations of each category are more similar and closer to each other than the observation of other categories. Fuzzy c-means is one of the clustering algorithms that assign observations to separate clusters with a specific degree of membership.

In these algorithms, an objective function is used as the evaluation index, that optimally clusters the existing observations. The fuzzy clustering algorithm was firstly proposed by Ruspini (Ruspini, 1969).

In this method, the degree of membership or belonging of each observation to each cluster, is determined through the membership matrix ($U = [u_{ij}]_{c\times n} = (\vec{u}_1; \vec{u}_2; \ldots; \vec{u}_n)$ where c is the number of clusters and n represent the number of observations).

Two constrains have been considered in FCM clustering method. First, no cluster should be null ($\sum_{j=1}^{u} u_{ij} > 0 \forall i \in \{1; \ldots; c\}$) and second, the normalization constrains that states the total degree of membership of each observation in all clusters should be equal one ($\sum_{j=1}^{u} u_{ij} = 0 \forall j \in \{1; \ldots; n\}$).

The FCM algorithm attempts to find partitions sets (c fuzzy clusters) for an observation group through minimizing the following objective function

$$J_f(X; U_f; C) = \sum_{i=1}^{c} \sum_{j=1}^{n} u_{ij}^{m} d_{ij}^{2} \quad (1)$$

where d_{ij} is the distance between jth observation, X_j and the center of the ith cluster and m $\in$ [1, ∞) denotes the degree of fuzziness (usually m=2). Therefore, if m tends to one ($m \to 1$), the clustering becomes the crisp method and if m tends to infinity (m$\to\infty$), the clustering becomes a fuzzy clustering. However, the J_f function cannot be minimized directly, and the iterative algorithms must be used. To solve this problem, the optimal steps are as follows:

1. Choosing appropriate values for m, c and selecting a small positive number for ε. We also fill the matrix C (the center of the clusters) randomly and set the value $t = 0$.
2. We calculate the membership matrix at $t = 0$ and then update at $t > 0$. Then the membership matrix, for fixed value of parameters is optimized as follows

$$u_{ij}^{(t+1)} = \frac{d_{ij}^{-2/(m-1)}}{\sum_{1=1}^{c} d_{1j}^{-2/(m-1)}} = \frac{1}{\sum_{1=1}^{c} \left(d_{1j}/d_{ij}\right)^{1/(1-m)}} \text{ for i} = 1, \ldots, \text{c and j} = 1, \ldots, \text{N} \quad (2)$$

In this equation, the degree of membership depends on the

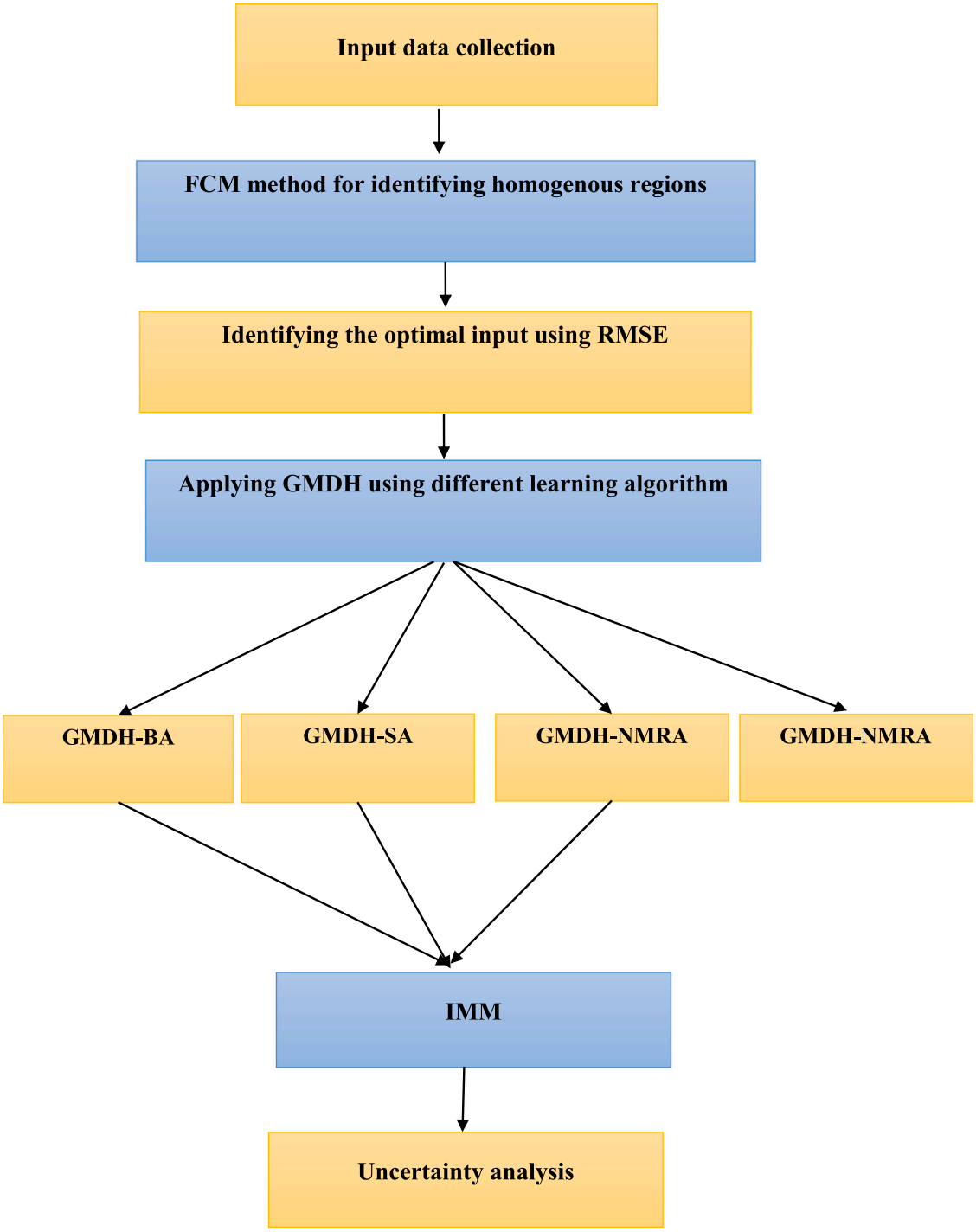

Fig. 2. Flowchart of methodology.

distance between an observation with the center of its cluster, and the distance with the center of other clusters.

$$c_i^{(t+1)} = \frac{\sum_{j=1}^{n} \left(u_{ij}^{(t+1)}\right)^m \overrightarrow{X}_j}{\sum_{j=1}^{n} \left(u_{ij}^{(t+1)}\right)^m} \text{for i} = 1, \ldots, \text{c} \quad (3)$$

3. In the final step, we update the membership matrix using the optimized membership degree.

The updating equation for the cluster centers depends on several parameters such as the location, shape, and size of the clusters. In addition to the mentioned parameters, the method of measuring the distance will be very sensitive.

4. Repeat steps 2 and 3 until $\left\|C^{(t+1)} - C^{(t)}\right\| < \varepsilon$ or $\left\|U^{(t+1)} - U^{(t)}\right\| < \varepsilon$ are established.

In practice, it has been shown that this method does not fall into local optimization. The FCM algorithm has been widely used as a clustering method in many studies.

Fig. 1 illustrates the three homogenous regions which was determined based on the FCM algorithm and Table 1 represents the crop and climatic information of each cluster located in these homogeneous regions.

Table 2
Different input scenarios for modeling BWF and GWF.

Scenario	Inputs for the BWF and GWF	RMSE for BWF (m3/kg)			RMSE for GWF (m3/kg)		
		Cluster1	Cluster2	Cluster3	Cluster1	Cluster2	Cluster3
1	All inputs except ETC	24	22	23	23	23	23
2	All inputs except IWR	22	24	25	-	-	-
3	All inputs except T_{max}	15	15	15	14	15	15
4	All inputs except T_{mean}	19	19	19	18	19	19
5	All inputs except P	21	23	23	20	20	20
6	All inputs except P_{eff}	14	14	14	16	15	14
7	All inputs except SH	15	16	16	16	14	15
8	All inputs except RH_{min}	17	18	19	19	18	18
9	All inputs except RH_{max}	15	15	12	15	17	14
10	All inputs except RH_{mean}	14	15	14	15	16	15
11	All inputs except WS	12	14	14	14	15	14
12	All inputs except Yield	25	27	28	22	22	24
13	All inputs	**12**	**11**	**12**	**11**	**12**	**11**

Bold number: The best input set for modeling

Table 3
Determining sample size percentages for training and testing.

	BWF			GWF		
	Training	Testing	RMSE	Training	Testing	RMSE
Cluster 1	50	50	19	50	50	17
	60	40	23	60	40	24
	70	30	12	70	30	11
	80	20	18	80	20	21
Cluster 2	50	50	22	50	50	17
	60	40	25	60	40	26
	70	30	14	70	30	12
	80	20	18	80	20	22
Cluster 3	50	50	25	50	50	17
	60	40	17	60	40	19
	70	30	11	70	30	12
	80	20	19	80	20	26

In cluster I, the climate type is moderate extra-arid (based on De Martonne classification (Rahimi et al., 2013)), average temperature is 18.40 degrees Celsius, average rainfall is 135.9 mm, average wind speed is 2.54 m/s, the sunshine hours is 9 h per day, the average humidity is 35.5%, and the saffron yield is 3.38 kg/ha.

Cluster II has cold arid climate type wherein average temperature is 15.99 degrees Celsius, average rainfall is 211.09 mm, humidity percentage is 43.7, average wind speed is 2.95 m/s, the sunshine hours is 8.6, and the saffron yield is 3.42 kg/ha.

In cluster III, climate type is cold semi-arid, average temperature is 15.63 degrees Celsius, average rainfall is 232 mm, average wind speed is 2.90 m/s, the sunshine hours is 8.2, the average humidity is 49.5%, and the saffron yield is 3.67 kg/ha.

2.3. WF computing

In this study, the BWF and GWF of the saffron product were calculated using the main framework described by Hoekstra and Chapagain (2008). In this regards, crop evapotranspiration, irrigation requirement and effective rainfall were calculated by applying the CropWat model in each plain of the study area.

The Penman-Monteith equation (Allen et al., 1998) has been used to calculate the evapotranspiration and the FAO-56 coefficients was considered to calculate crop evapotranspiration. For more details, one can refer to Allen et al. (1998).

In this study, the CropWat tool using the crop coefficients (Kc) proposed by Shahidi et al. (2020); Keykhamoghadam et al. (2013) was applied and the ETc was calibrated for each saffron cultivation area.

Then, the net irrigation requirement was calculated from the difference of evapotranspiration with the effective precipitation. The water requirement was also calculated using the irrigation efficiency (reported by the Ministry of Agriculture for each region). After determining the variables affecting the product, the BWF and GWF were calculated.

Green water is a part of effective rainfall that is consumed by plants in an unsaturated soil environment (Bazrafshan et al., 2019a). The green water footprint is computed using the following equation.

$$GWF = \frac{(P_e) * 10}{Y} \tag{4}$$

where, GWF is green WF in cubic meters per ton; P_e denotes the total effective rainfall (using USDA S.C. Method) during the plant growth period in millimeters and Y is the yield of saffron in ton per hectare.

Blue water involves the underground water and surface runoff from rains and lakes water that collects behind the dams and are used in the irrigation sector. (Bazrafshan et al., 2019b) The BWF is calculated using the equation

$$BWF = \frac{(ET_c - P_e) * 10}{Y} \tag{5}$$

where BWF is the blue WF in cubic meters per ton and ET_c represents the crop evapotranspiration in millimeter.

2.4. Structure of group method of data handling

The group method of data handling (GMDH) model is a machine learning algorithm proposed by Ivakhnenko (1971). The GMDH is used to analyze complex and non-linear systems without pre-assumptions about internal parameters.

GMDH is a multilayer perceptron neural network (MLP) that constructs the successive layers with connections. GMDH analyses data using polynomial transfer activation functions such that the layers and neurons are determined automatically. The mathematical function of GMDH is as follows (Mahdavi-Meymand and Zounemat-Kermani, 2020):

$$y = b_0 + \sum_{i=1}^{m} b_i x_i + \sum_{i=1}^{m}\sum_{j=1}^{m} b_{ij} x_i x_j + \sum_{i=1}^{m}\sum_{j=1}^{m}\sum_{k=1}^{m} b_{ijk} x_i x_j x_k \tag{6}$$

Where $y$is the response variable,b_0, b_{ij},$b_i$and b_{ijk} rare the model weighting coefficients, x_i, x_k, and $x_j$are the predictors, and m denotes the number of input (predictor) variables. This study used the quadratic form of the polynomial function. Therefore, Equation 6 is reduced to the Equation 7 which is expressed as below (Mahdavi-Meymand and Zounemat-Kermani, 2020).

$$y = b_0 + b_1 x_1 + b_2 x_2 + b_3 x_1^2 + b_4 x_2^2 + b_5 x_1 x_2 \tag{7}$$

According to estimation parameters in regression models, the weighting coefficients vector of GMDH can be estimated as (Ivakhnenko,

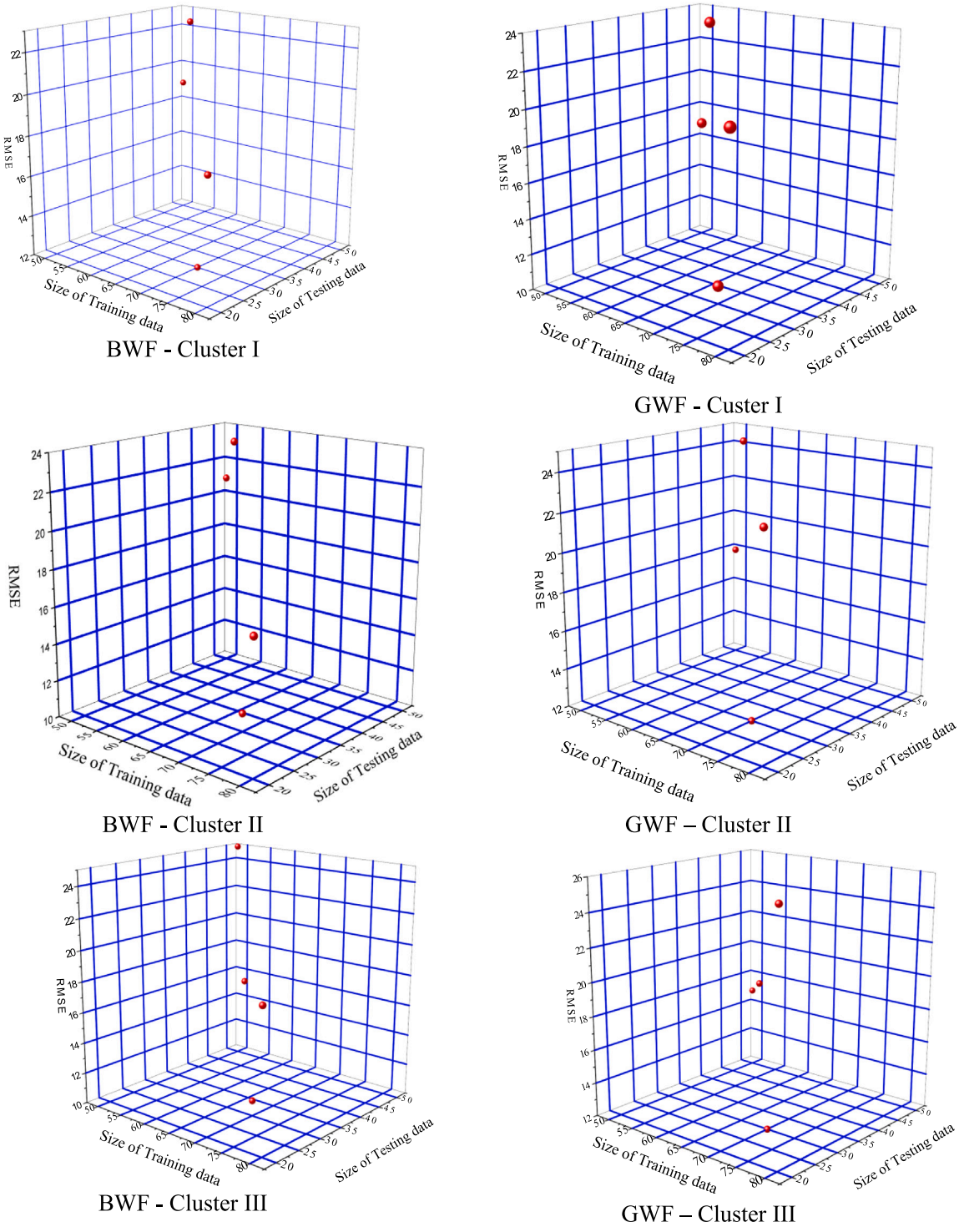

Fig. 3. Determining sample size for training and testing stages based on GMDH NMR.

1971).

$$b = \left(A^T A\right)^{-1} A^T y \tag{8}$$

Where *A* is the matrix of observations in the following form (Ivakhnenko, 1971).

$$A = \begin{bmatrix} 1 & x_1^1 & x_2^1 & x_1^1 x_2^1 & \left(x_1^1\right)^2 & \left(x_2^1\right)^2 \\ 1 & x_1^2 & x_2^2 & x_1^2 x_2^2 & \left(x_1^2\right)^2 & \left(x_2^2\right)^2 \\ . & . & . & . & . & . \\ 1 & x_1^m & x_2^m & x_1^m x_2^m & \left(x_1^m\right)^2 & \left(x_2^m\right)^2 \end{bmatrix} \tag{9}$$

The next layer neurons of GMDH model is calculated as

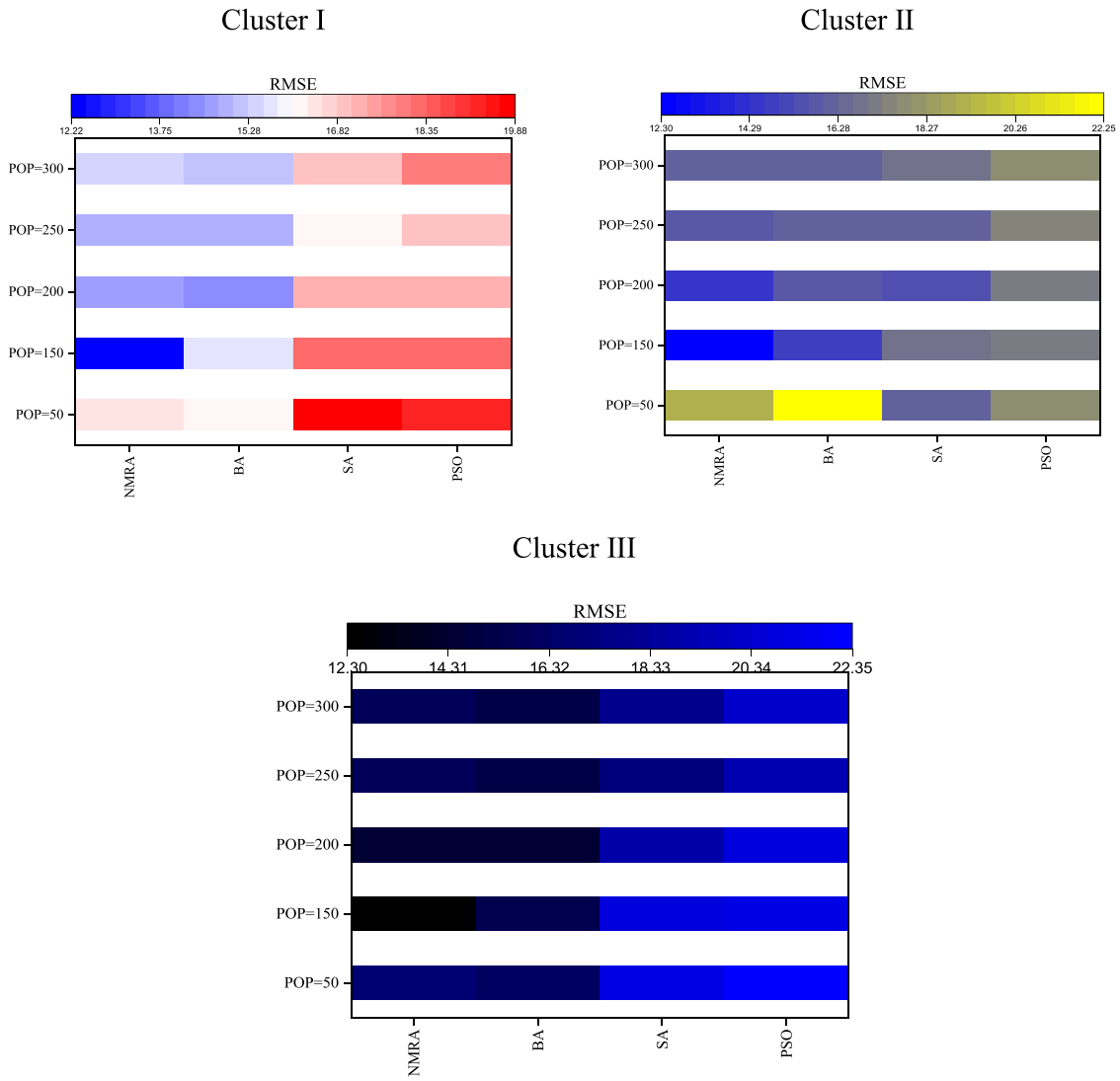

Fig. 4. F Sensitivity Analysis of population size (POP) for various algorithms in predicting BWF.

Table 4
The sensitivity analysis of random parameters.

	Parameter	BWF	GWF
		Maximum number of iterations	
Cluster 1	NMRA	150	150
	BA	200	250
	SA	300	300
	PSO	400	400
Cluster 2	NMRA	150	150
	BA	200	250
	SA	300	300
	PSO	400	400
Cluster 3	NMRA	150	150
	BA	200	250
	SA	300	300
	PSO	400	400

Iteration: Random parameter

$$N_n = \binom{N_{np}}{2} \tag{10}$$

where N_{np} is the number of neurons in the current layer. In GMDH, the neurons are added layer by layer. In order to avoid the complexity of the GMDH model, the maximum number of neurons may in each layer is determined based on the pressure criteria (Mahdavi-Meymand and Zounemat-Kermani, 2020).

$$e_c = w \times RMSE_{best} + (1 - w) \times RMSE_{worst} \tag{11}$$

where e_c is the selection pressure parameter, $RMSE_{best}$ is the RMSE of the best neuron, and$RMSE_{worst}$ denotes the RMSE of the worst neuron. Equation (11) will remove some neurons from the structure of the GMDH.

2.5. Naked mole rate algorithm (NMRA)

Salgotra and Singh (2019) introduced the NMRA optimization algorithm, which was developed based on the mating pattern of NMRs. The group of NMRs consists of 295 individuals. In this group, Queens leads the group and divides members into breeders and workers.

Breeders are selected for mating while workers carry out other duties. The best workers replace the breeders. At the first stage, the NMRs population is generated as follows:

$$NM_{i,j} = NM_{\min\ ,j} + U(0,1) \times \left(NR_{\max\ ,j} - NR_{\min\ ,j}\right) \tag{12}$$

where $NM_{i,j}$ is the ith solution in the jth dimension, $NR_{\max\ ,j}$denotes the upper bound of the decision variable, $NR_{\min\ ,j}$represents the lower bound of the decision variable and $U(0,1)$is a random number taken from the

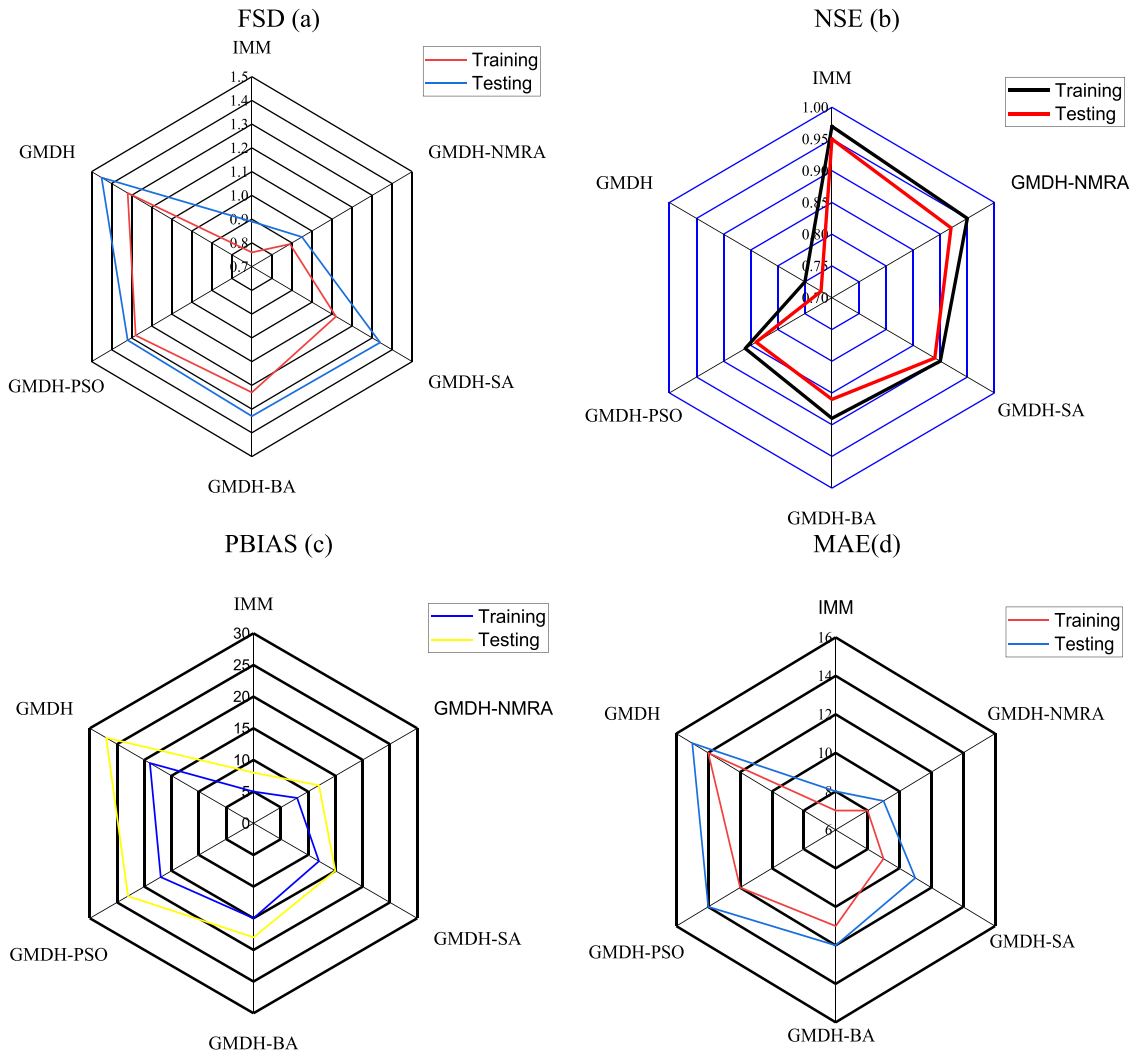

Fig. 5. Radar plots of optimizing algorithms in modeling BWF.

uniform distribution. After initialization, the objective function is calculated. The objective function is used to divide the population into workers and breeders. Now, two stages should be considered:

1) Worker Phase: At this stage, workers attempt to improve their skills. They strive to become a breeder for mating with the queen. The objective function of the new NMR is determined and will be saved if it is a better objective function. The following equation is used to provide the new NMRS in this stage:

$$wo_i^{t+1} = wo_i^t + \lambda\left(wo_i^j - wo_t^k\right) \tag{13}$$

where wo_i^{t+1} denotes the ith worker in the (t + 1)th iteration, wo_t^jrepresents the ith worker in the t th iteration, λ denotes the mating factor, and wo_t^k is a random solution that is selected from the worker's pool.

2) Breeder phase: Breeders must also strive to update themselves to remain breeders and to be selected for mating. when breeders cannot update fitness information, they may be pushed back to the worker group. The following equation updates the breeders at (t + 1)th iteration.

$$br_i^{t+1} = (1-\lambda)br_i^t + \lambda\left(d - br_i^t\right) \tag{14}$$

where br_i^{t+1}denotes the ith breeder in the (t + 1)th iteration and $d$is the best solution. It is assumed that there is only one queen such that the best breeder mates with it. The algorithm identifies breeders and workers. The breeders and workers are selected based on an initial evaluation. Workers' fitness is updated such that they may improve and gain the opportunity to be breeders. Breeders update themselves to remain breeders. The best breeders are considered as the candidate solutions.

2.6. Structure of Bat algorithm (BA)

This algorithm was inspired from the Bat (BA) life. The advantages of BA algorithm involve fast convergence, high flexibility, and high accuracy. BA has been applied in different fields, such as training soft computing models (Lu et al., 2021), numerical optimization (Wang et al., 2019), optimal reactive power dispatch (Mugemanyi et al., 2020), optimal feature selection (Al-Dyani et al., 2018), energy-efficient clustering (Bacanin et al., 2022), and reservoir operation (Shourian and Jamshidi, 2022). Echolocation ability helps bats to identify food and obstacles. Bats randomly fly with velocity V_i at location X_i, frequency F_i, wavelength λ, and loudness A_0. Bats update their location, velocity, and frequency based on the following equations

$$F_i = F_{mn} + (F_{\max} - F_{\min})\beta \tag{15}$$

$$V_i^t = V_i^{t-1} + \left(X_i^{t-1} - X^*\right)F_i \tag{16}$$

$$X_i^t = X_i^{t-1} + V_i^t \tag{17}$$

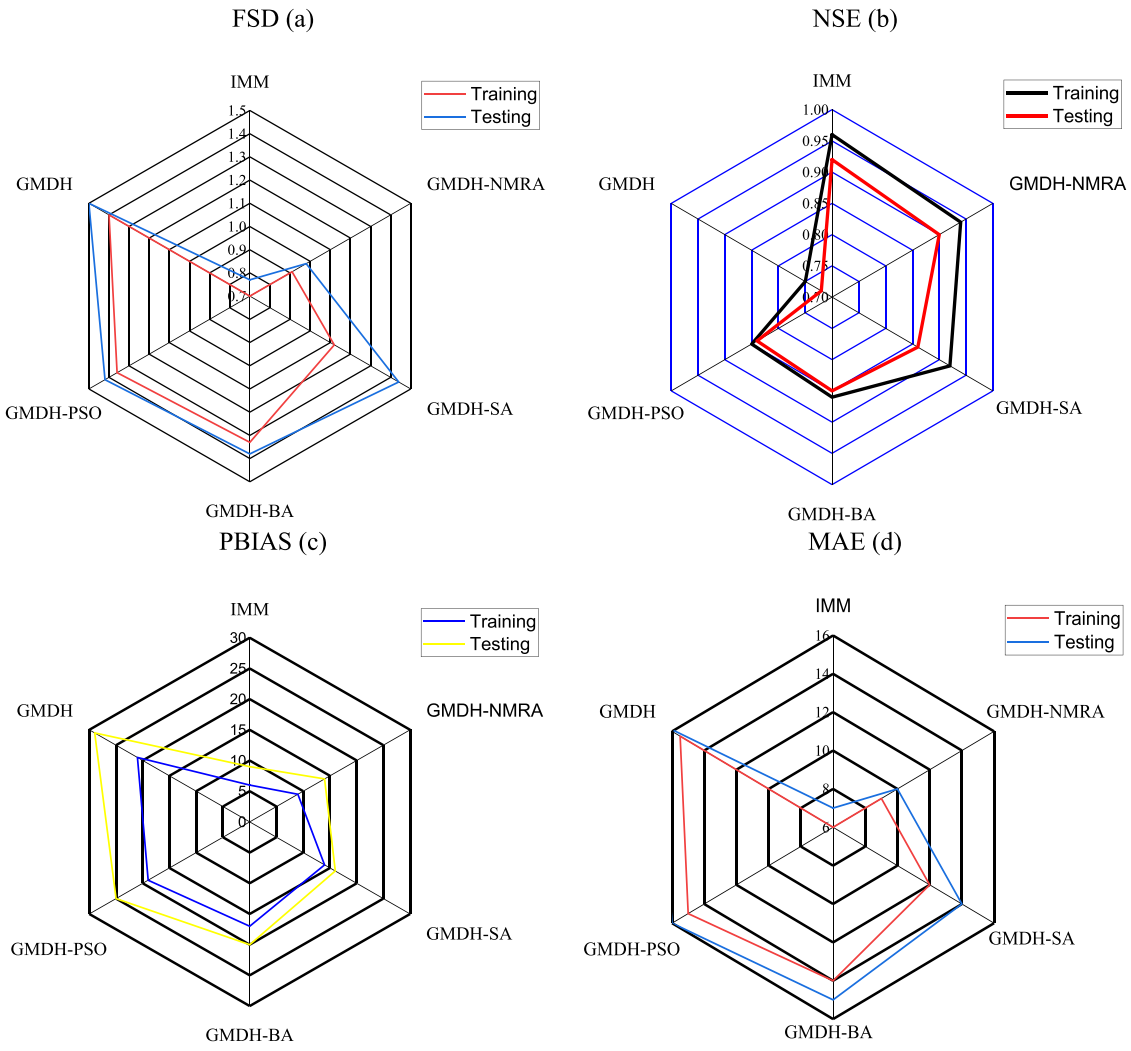

Fig. 6. Radar plots of optimizing algorithms in modeling GWF.

where $F_i$denotes the frequency of ith bat, $F_{\max}$ and $F_{\min}$are the maximum and minimum frequency respectively, V_i^t represents the velocity of ith bat, t is number of iteration, X^*indicates the best location of bat, X_i^tdenotes the location of ith bat and β is a random number. Bats perform local search based on the random walk method as below (Bacanin et al., 2022):

$$X_{new} = X_{old} + \varepsilon A^t \tag{18}$$

where X_{new} denotes the new location of bats, $X_{old}$is the old location of bat, and A^t indicates the loudness. A balance between exploration and exploitation is maintained by adjusting the pulsation rate and loudness denoted in the following expressions.

$$A_i^{t+1} = \alpha A_i^t \tag{19}$$

$$r_i^{t+1} = r_i^0[1 - \exp(-\gamma t)] \tag{20}$$

Where A_i^{t+1}denotes the loudness of ith bat at iteration t + 1, $r_i^0$is the initial pulsation rate, and γ and $\alpha$are the constant terms.

2.7. Structure of shark algorithm (SA)

The shark algorithm was inspired from shark life. Abedinia et al. (2016) proposed SA for solving complex problems. Applying the rotational movement of the sharks reduces the possibility of falling the SA algorithm into the local optimization. SA algorithm has been applied in various fields, such as training soft computing models (Seifi et al., 2020), medical image enhancement (Zhou et al., 2020), fingerprint authentication (Ahmed and Abdulhameed, 2020), estimating groundwater level (Rezaei et al., 2021), and reservoir operation (Ehteram et al., 2021). Sharks use their olfactory sense to locate prey. When they get closer to their prey, they smell more strongly. The SA operates based on the following assumptions:

1) Sharks consider wounded fish to be prey. Blood is injected into the water when the fish is wounded.
2) Continuously, blood is injected into the ocean, and the impact of water flow is ignored.
3) In the search space, there is only one fish.

Sharks vary their speed from a minimum to a maximum. However, a speed limiter is considered for updating the shark's velocity (Ehteram et al., 2021):

$$\left|ve_{i,j}^k\right| = \min\left[\left|\varsigma_k.r_1.\frac{\partial(OF)}{\partial x_j}\right| + \alpha_k.r_2.ve_{i,j}^{k-1}\right|, \left|\delta.ve_{i,j}^{k-1}\right|\Bigg] \tag{21}$$

where $ve_{i,j}^k$ denotes the velocity of ith shark in jth dimension, K is the number of stages, r_1, and r_2 are the random numbers, $\delta$is the speed limiter, $\alpha_k$represents the inertia coefficient, and $\varsigma_k$is a random number and OF denotes the objective function. The sharks update their location

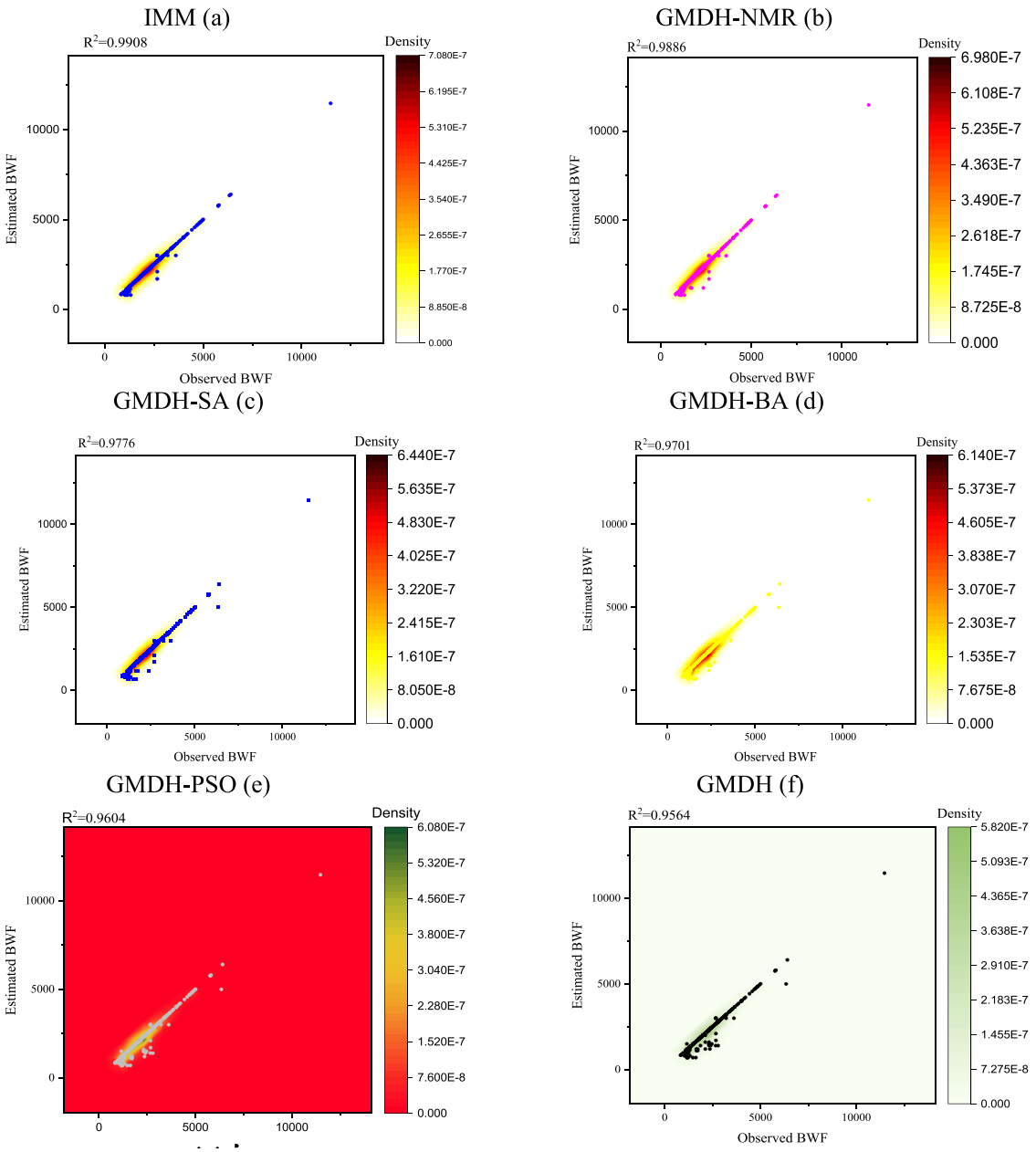

Fig. 7. The heat scatter plots for predicted and observed BWF (Cluster I).

as follows:

$$Y_i^{k+1} = X_i^k + \Delta t_k \tag{22}$$

where Y_i^{k+1}denotes the location of the shark after the forward movement, Δt_krepresents the time interval and $X_i^k$is the location of ith shark in the kth stage. With the rotational movement, the SA achieves the best location. Sharks typically perform rotational movements and forward movements to improve their movement direction. Sharks rotate on a closed contour, not necessarily a circle. Shark performs local search in each stage to find better candidates for optimization

$$Z_i^{k+1,m} = Y_i^{k+1} + r_3 . Y_i^{k+1} \tag{23}$$

Where r_3 is the random number, m: (m=1. to M) represents the number of points in the local search at each stage, and $Z_i^{k+1,m}$denotes the location of sharks after rotational movement. For a maximization problem, the final location is obtained as follows:

$$X_i^{k+1} = \arg(\max)\left\{OF\left(Y_i^{k+1}\right), OF\left(Z_i^{k+1}\right), OF\left(Z_i^{k+1,M}\right)\right\} \tag{24}$$

2.8. Structure of particle swarm optimization (PSO)

PSO is a robust optimization algorithm that is used for solving complex problems. The key advantages of the PSO algorithm are easy implementation, fast convergence, high accuracy, parallel computation, and high flexibility for coupling with various models (Kashani et al., 2021). First, the initial locations and velocities of the particles are initialized. Next, the objective function is computed to determine the optimal solution. This solution leads the other solutions toward the best location (Wang et al., 2021). The location and velocity of particles are updated according to the following equations, and the process continues until a stop condition is met (Wang et al., 2021).

$$v_{id}^n = \omega v_{id}^n + \phi_1 rand_1\left[p_{id}^n - x_{id}^n\right] + \phi_2 rand_2\left[g_{id}^n - x_{id}^n\right] \tag{25}$$

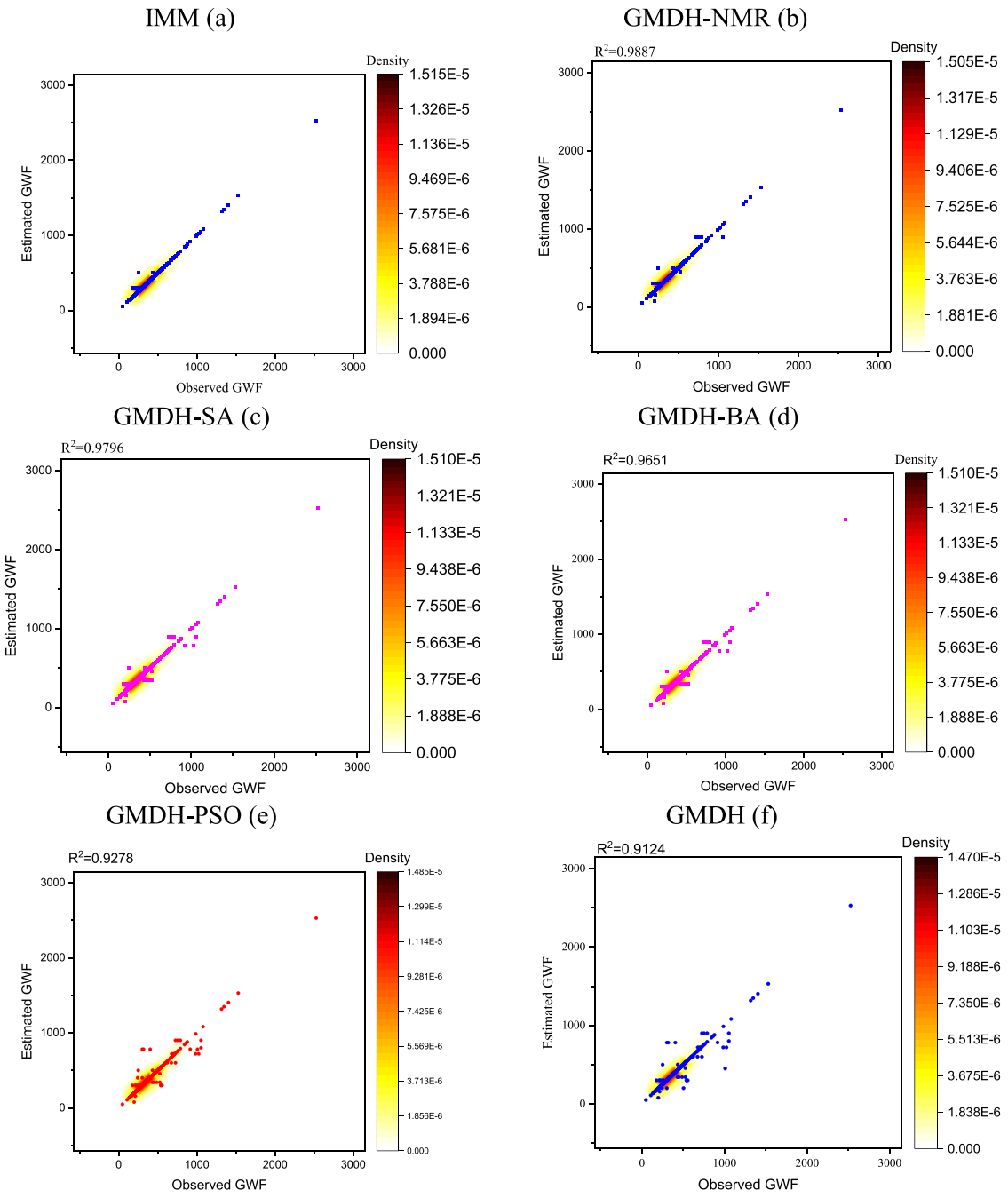

Fig. 8. The heat scatter plots for predicted and observed GWF (cluster I).

$$x_{id}^{n+1} = x_{id}^{n} + v_{id}^{n+1} \quad (26)$$

where n is the number of iterations, d is the number of dimensions, $\phi_1 and \phi_2$ denote the acceleration coefficient, p_{id}^{n} represents the local best solution, g_{id}^{n} is the global best solution, $rand_1$ and $rand_2$ are the random numbers, v_{id}^{n+1} denotes the velocity of the ith particle in (n + 1)th iteration and x_{id}^{n+1} represents the location of the ith particle.

2.9. Structure of inclusive multiple models (IMM)

The Inclusive Multiple Model is an ensemble model that improves the accuracy of individual models. Shabani et al. (2021) indicated that the IMM model has a good performance in predicting CO_1 emission. They applied the outputs of several individual models as the inputs of the IMM. Khatibi and Nadiri (2021) stated that the IMM model uses the advantages of multiple models and improves the efficiency of individual models. Jalil-Masir et al. (2022) applied the IMM model as a collaborative model. In this study, the IMM model was used in order to improve the accuracy of the optimized GMDH models as follows:

The individual GMDH NMRA, GMDH-SA, GMDH-BA, and GMDH are applied in order to predict the output variables in the first stage. Then, the outputs of the previous stage are used as the inputs of the GMDH model. The GMDH in the second stage integrates and combines the outputs of various models.

2.10. Generalized likelihood uncertainty estimation (GLUE)

GLUE is a useful approach for quantifying the uncertainty in the modeling process. GLUE has been applied in various fields, such as un-

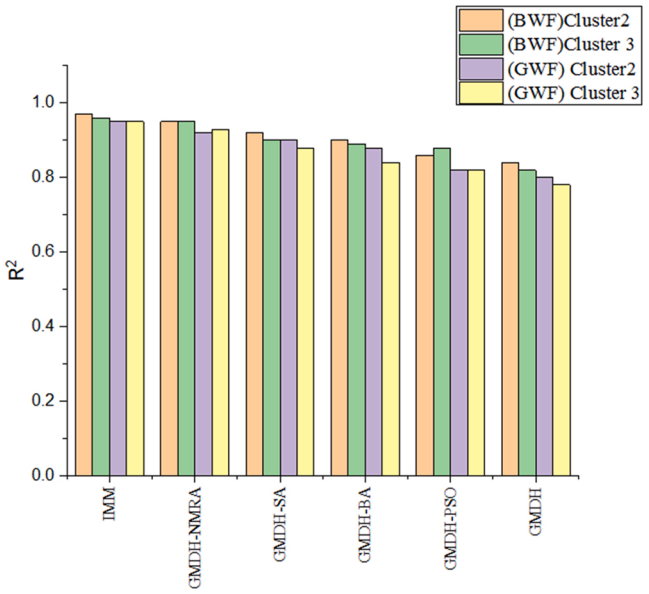

Fig. 9. The coefficient of determination (R^2) between predicted and observed GWF and BWF (Clusters II& III).

certainty analysis of discharge (Maghrebi and Vatanchi, 2021), reservoir operation (Muronda et al., 2021), hydrological model uncertainty (Zuo et al., 2021), uncertainty quantification of eruption (Constantinescu et al., 2022), and urban flood model (Kobarfard et al., 2022). According to the following steps, the input and parameter uncertainties are quantified:

1. In the first step the prior distribution of input parameters is determined. Typically, the normal distribution is used for input parameters. However, it cannot be used as a prior distribution for model parameters. The parameters fluctuate during the training step, which demonstrates the parameter properties. In this study, 4000 GMDH models are trained to estimate the probability distribution of ANN parameters. This training number was selected because the parameters remained unchanged between 1000 and 4000 GMDH models.
2. The prior distribution using the Monte Carlo method provides N samples.
3. The GMDH models are run using the generated parameters in the previous step.
4. The likelihood function is determined. The Nash-Sutcliffe efficiency is used as the likelihood function (McCuen et al., 2006):

$$P(L|\theta_i) = 1 - \frac{\sum_{o=1}^{O}[l_o - \widehat{l}_o(\theta)]}{\sum_{o=1}^{O}([l_o - \bar{l}_o])^2} \quad (27)$$

Where $P(L|\theta_i)$is the likelihood function, $l_o$denotes the observation value, $\bar{l}$represents the oth simulated value using parameter sets θ and $\bar{l}$denotes the average of observed value.

5. A threshold is considered and the parameters with a likelihood blow threshold are discarded, whereas other parameters are used.
6. The posterior probability is obtained as follows:

$$p(\theta_i|L) = \frac{p(\theta_i).p(L|\theta_i)}{\sum_{i=1}^{N} p(L|\theta_i)} \quad (28)$$

where $p(\theta_i|L)$denotes the posterior probability.

The mean and variance of the parameters are computed. Fig. 2 displays the methodology flowchart.

3. Result

3.1. Selecting the best input scenario

In this research, in order to select the best input scenario (introduced in Table 2), the RMSE criterion based on the GMDH NMRA algorithm was considered. The lowest RMSE indicates the best input.

The input scenarios for GWF and BWF are displayed in Table 2. According to the results, the lowest RMSE and the best results in all three clusters and both predictive variables, belongs to the scenario 13, in which all predictors are included into the model.

In regards with GWF, the highest value of RMSE belongs to the scenarios 1 and 12, in which the inputs contain all variables except ETC and Yield. Therefore, the GWF is highly correlated with ETC and Yield.

Like the GWF, the highest RMSE in predicting BWF belongs to the scenarios 1 and 12, whose input involves all variables except the Yield and ETc. Further, in both cases the lowest RMSE produced by a scenario that involves all predictors.

3.2. Determining the sample size

Determining the sample size for training and testing parts is very important in modeling. In this research, the RMSE was used to determine the appropriate sample size of the data. The best sample size is one that minimizes the RMSE in both training and testing steps.

Table 3 represents the error rate RMSE versus the sample size for the testing and training stages for BWF and GWF in all three clusters. According to the results, assigning 70% and 30% of observations respectively to the training and testing sets produced the lowest RMSE in all three clusters. Therefore, in order to modeling BWF and GWF in all three clusters, observations were separated into 70% and 30% for the training and testing purpose respectively (Fig. 3).

3.3. Selecting appropriate random parameters

Fig. 4 illustrates the RMSE versus different population sizes (POP) for NMRA, BA, SA and PSO algorithms in modeling BWF in all three clusters. Each algorithm involves various random parameters, such that the population size is an important random parameter. Sensitivity analysis means changing the population size versus the objective function in order to achieve the best population size. The objective function in the present study is the RMSE and the best population size is one that produces the lowest RMSE value.

The objective function in cluster 1 based on the NMR algorithm and for population sizes POP= 50, POP= 100, POP= 200, POP= 250 and POP= 300 were 16.55, 12.23, 14.55, 15 and 15.5, respectively. Therefore, the best population size for the NMR algorithm is POP= 150 with the value 12.23 of objective function.

The objective function for BA with respect to POP= 50, POP= 100, POP= 200, POP= 250 and POP= 300 was 16.12, 15.54, 14.35, 14.78 and 15.23, respectively. Therefore, the best population size for BA is POP= 200 that produced the lowest RMSE= 14.35.

Further analysis indicated that the NMR algorithm has the best performance in cluster I such that it produced the lowest RMSE= 12.23 for population size POP= 150. In clusters II and III, the best population size was investigated in different algorithms, and the NMRA algorithm produced the lowest RMSE= 12.34 for the population size POP= 150.

Table 3 represents large number of iterations for various algorithms in modeling BWF and GWF in all three clusters. Since the iteration number is another important parameter in evolutionary algorithms, sensitivity analysis is performed to calculate the maximum iteration number. In order to achieve the best value of the objective function, the parameter of maximum iteration such as the population size is changed. The best value of maximum iteration number for each algorithm are provided in Table 4.

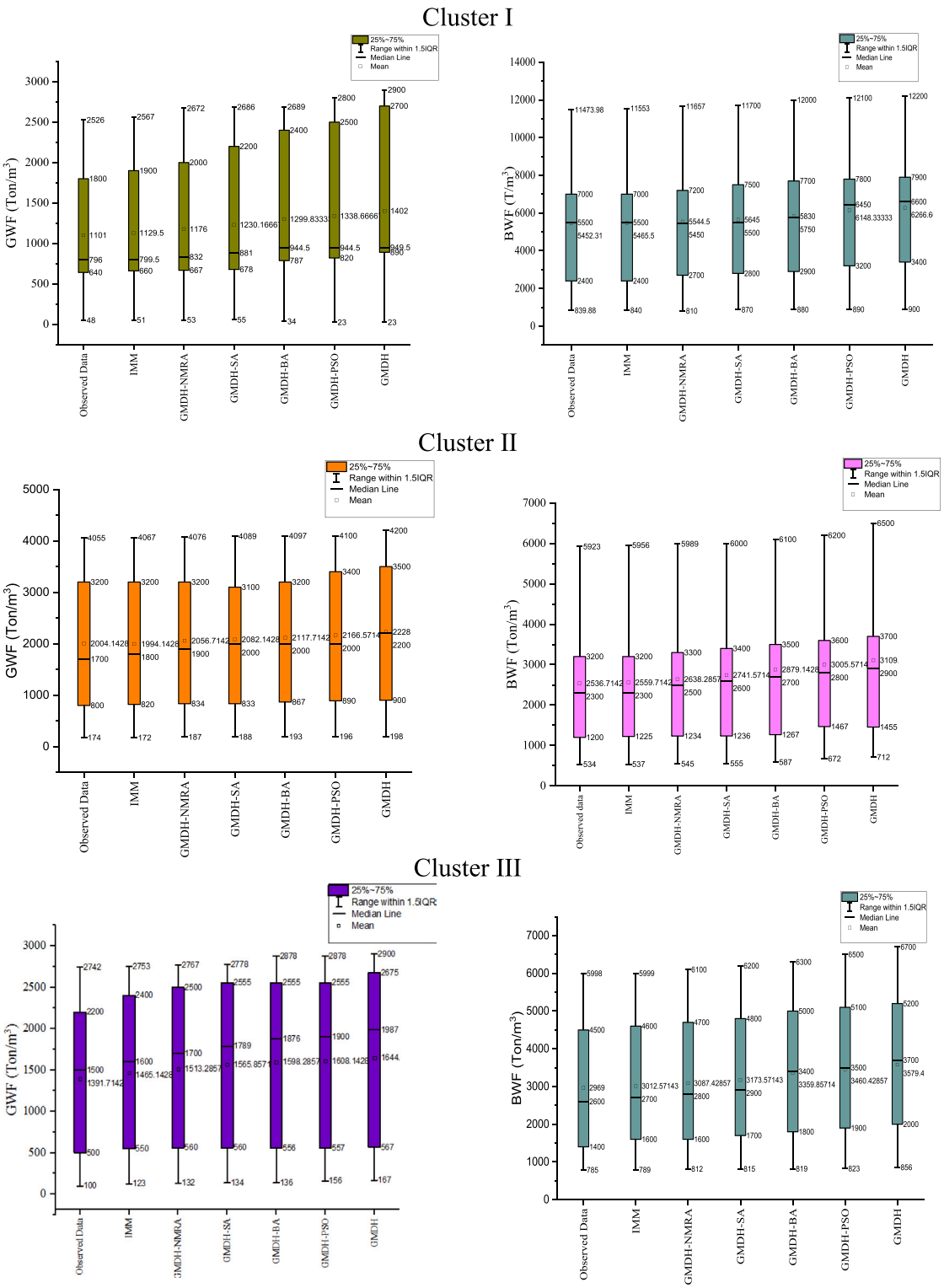

Fig. 10. Boxplot of the observed and predicted BWF and CWF based on the testing observations in Clusters I & II & III.

3.4. Graphical assessment of model accuracy

Fig. 5 illustrates the radar plot of comparing model accuracy based on the FSD, NSE, PBIAS and MAE criteria for modeling BWF. Fig. 5a indicates the radar plot based on the FSD value.

The training FSD for IMM, GMDH NMRA, GMDH-SA, GMDH-BA, GMDH-PSO and GMDH algorithms were 0.76, 0.89, 1.12, 1.23, 1.28 and 1.32, respectively. Fig. 6b illustrates the NSE values of modeling BWF.

The testing NSE for IMM, GMDH NMRA, GMDH-SA, GMDH-BA, GMDH-PSO and GMDH algorithms were 0.95, 0.92, 0.89, 0.86, 0.84 and 0.72, respectively.

The testing PBIAS for IMM, GMDH NMRA, GMDH-SA, GMDH-BA, GMDH-PSO and GMDH algorithms were 8, 12, 15, 18, 23, 27 respectively (Fig. 6c). Fig. 6d illustrates the radar plot MAE criterion.

The training MAE for IMM, GMDH NMRA, GMDH-SA, GMDH-BA, GMDH-PSO and GMDH algorithms were 8, 9, 11, 12, 14 and 15,

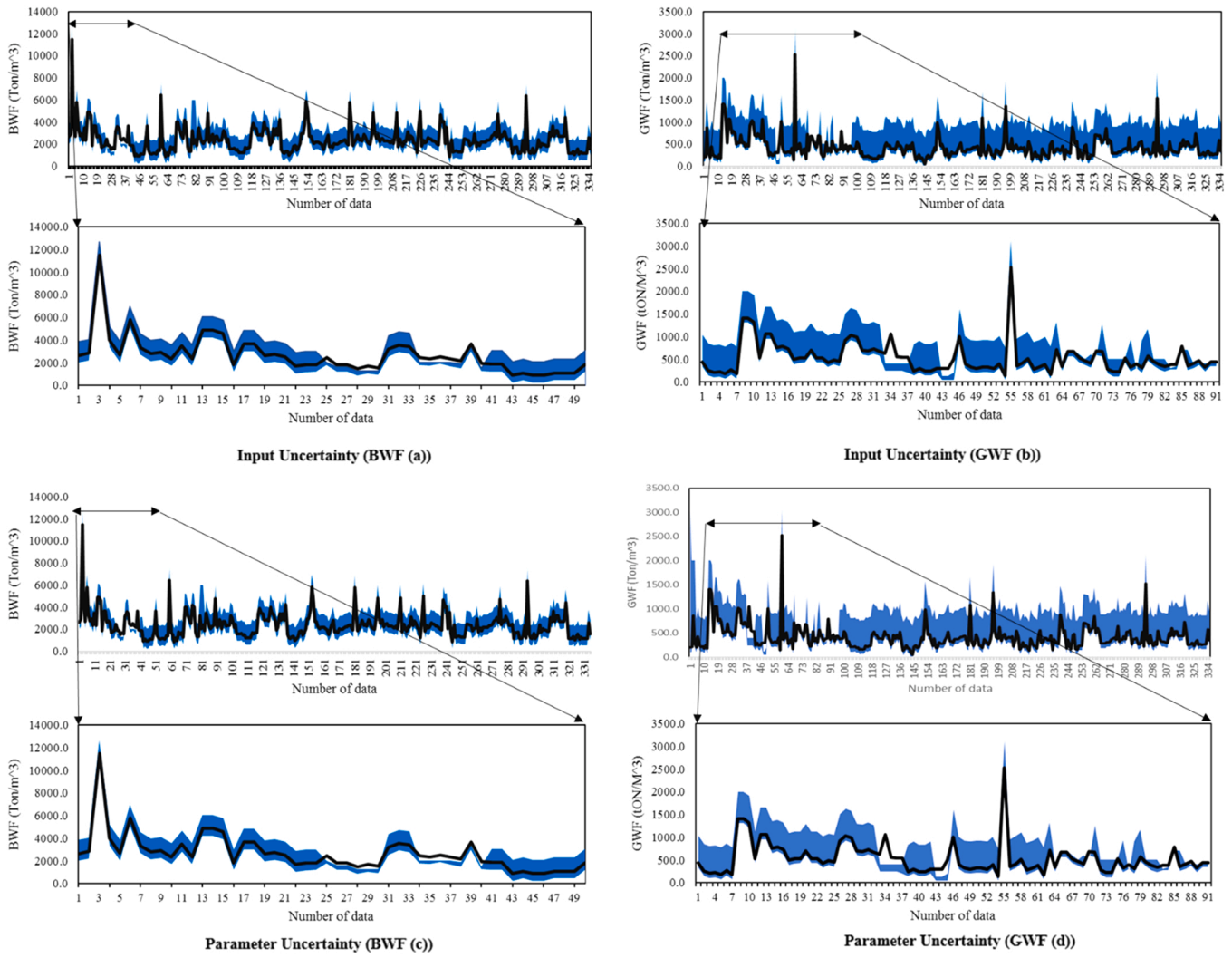

Fig. 11. Uncertainty analysis caused by the inputs and parameters for BWF (a, c) and for GWF (b, d) in cluster I.

respectively. According to all assessment criteria, the IMM algorithm was the best compared to the alternatives. Results of this section indicate that the evolutionary algorithms increase the accuracy of the GMDH model.

The hybrid GMDH models have different accuracies. In this regard, the NMRA algorithm had the best and the PSO algorithm had the lowest accuracy than the other optimization algorithms. Since the IMM used the outputs of several individual models, it had better accuracy than the individual GMDH models. Therefore, using the IMM model has improved the results.

Fig. 6 represents the radar plots of FSD (Fig. 6c), NSE (Fig. 6b), PBIAS (Fig. 6a) and MAE (Fig. 6d) criteria for modeling GWF. Similarly, the results of modeling BWF, the IMM model produced the lowest error rate than the alternatives in modeling GWF, so that the optimized GMDH had better performance than the individual GMDH model.

Scatter plot is a useful tool for evaluating the accuracy of predicted models. When the data overlaps, the heat scatterplot helps to identify the number of observations in a specific area. Figs. 7 and 8 denote the scatter plot of prediction BWF and GWF in cluster I.

Fig. 7(a-f) represents the scatter plot between predicted and observed BWF. The estimated R^2 for IMM, GMDH NMRA, GMDH-SA, GMDH-BA, GMDH-PSO and GMDH models are 0.99, 0.98, 0.97, 0.97, 0.96 and 0.95, respectively. Therefore, based on the R^2 criterion, the IMM model is more accurate than the alternatives.

Fig. 9(a-f) denotes the scatter plot of predicted versus the observed GWF. As results show, the highest R^2 was produced by IMM model. Therefore, the IMM model has higher accuracy in prediction both variables in cluster I.

Fig. 9 represents the barplot of R^2 value for predicted GWF and BWF in clusters II and III. According to the results, the IMM model produced the highest R^2 between the estimated and observed BWF and GWF in both clusters. Therefore, due to the use of the outputs of several individual models, the IMM has the highest accuracy among the alternatives in all three clusters.

3.5. Graphical assessment of model performance

In order to evaluate the performance of the models, the boxplot of the estimated and observed GWF and BWF was used. Fig. 10 compares of the boxplot of the predicted and the observed BWF and GWF for saffron in 3 clusters.

Cluster I: In this cluster, the IMM model performed very well in estimating the dispersion indices of observed GWF including median (799.5), maximum (2567), minimum (51), first quartile (660) and third quantile (1900). Compared to the other hybrid models, the GMDH NMRA also estimated the dispersion indices very well however, it ranks after the IMM in terms of efficiency.

As figure shows, the median, the first and the third quartiles of IMM boxplot in estimating BWF are 5500, 2400, and 7000 ton/m^3, respectively, which completely closed to the observed values. The maximum (

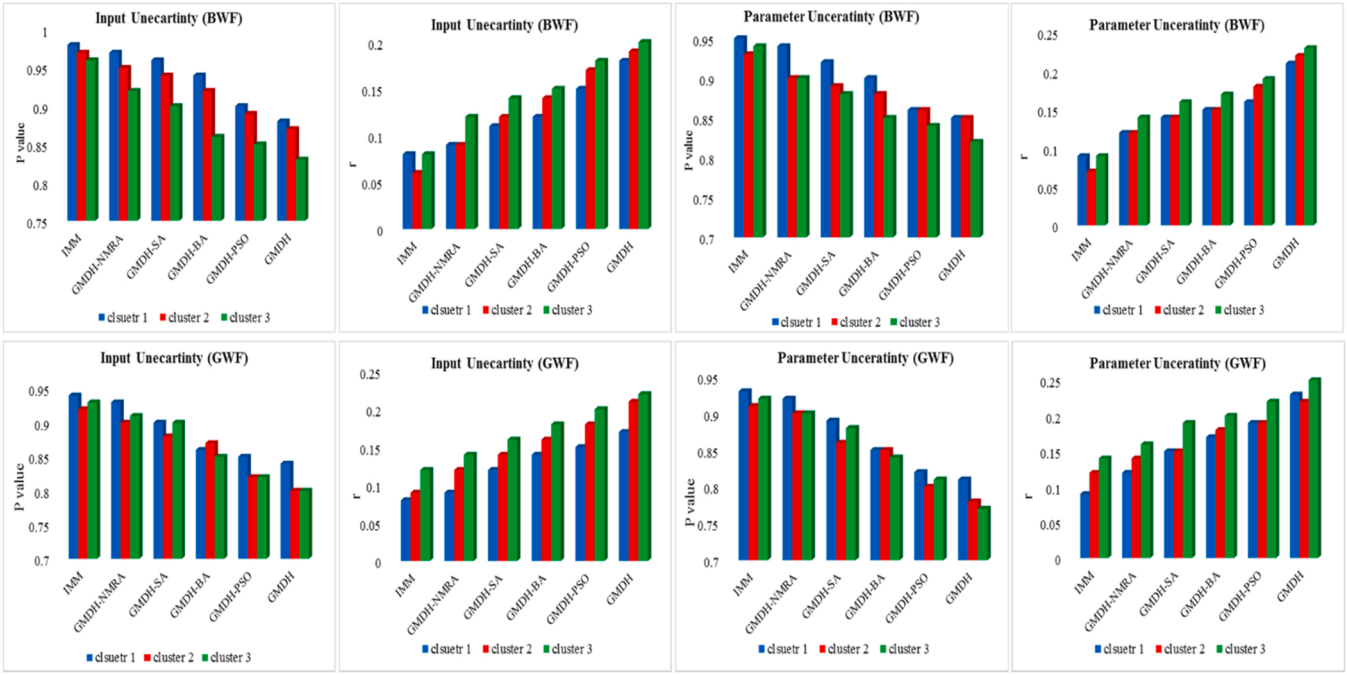

Fig. 12. Uncertainty analysis in all clusters.

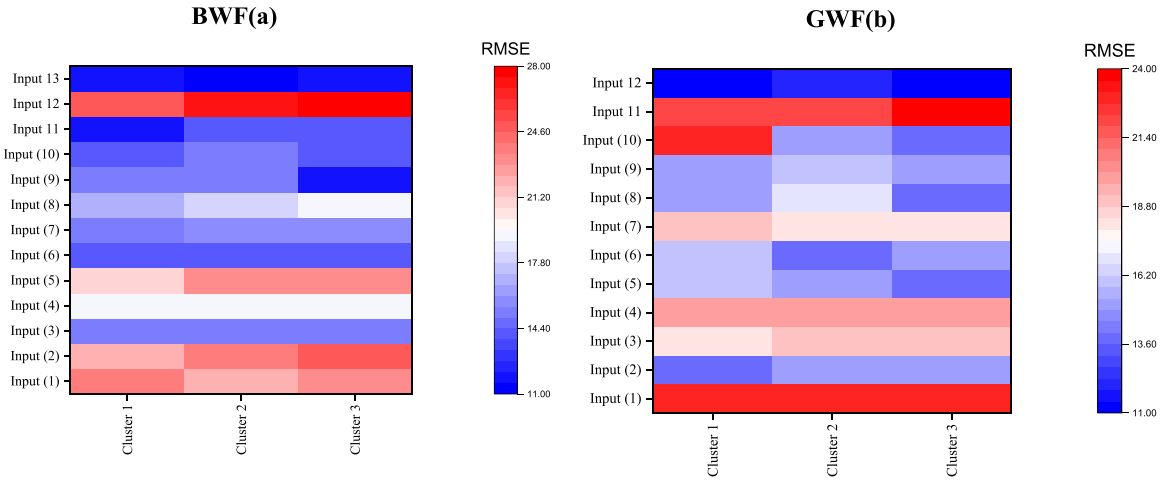

Fig. 13. Variation of RMSE for selection of the best inputs for predicting BWF (a) and GWF (b) based on GMDH NMR (scenarios provided in Table 1).

11,553) and minimum (840) values of the IMM boxplot are also closed to the observed BWF values. The other models are highly deviated from the observed BWF dispersion indices.

Cluster II: The estimated median (2300 ton/m3) and third quantile (3200 ton/m3) of the BWF by the IMM model is very closed to the observed values. Further, there is the highest agreement between the first quartile (1225), the minimum (537) and the maximum (5956) of observed BWF and the predicted values by the IMM model.

In addition, the IMM model has performed very well compared to the other hybrid models in estimating the median (1800), maximum (4067) and minimum (172) of the observed GWF. This model also estimated the third quartile (3200) of GWF very accurately.

Cluster III: The IMM model has the best performance compared to the alternatives with the most similarity of estimated to the observed BWF and GWF. This model also estimated the maximum (5999) and minimum (789) of BWF as well as the maximum (2753) and minimum (123) of GWF very accurately. The estimated values by the other hybrid models are significantly deviated from the observed BWF and GWF.

3.6. Uncertainty analysis caused by the parameters and inputs on estimating WF saffron

Uncertainty in the modeling process is dependent to the inputs and parameters. In the present study, the uncertainty caused by the parameters and inputs is analyzed separately.

Figs. 11a, 11b, 11c and 11d illustrate the uncertainty due to the inputs and parameters in predicting BWF and GWF variables.

More observation points within the confidence region indicate the lower uncertainty. Also, the smaller band of the confidence region represents the lower uncertainty. According to Figs. 11a and 11c, the uncertainty caused by the inputs is less than the uncertainty caused by the parameters. For instance, in predicting GWF, the p value due to the inputs and parameters uncertainty is 0.98 and 0.95 respectively (Fig. 11a). Figs. 11b and 11d also indicate that the uncertainty caused by inputs is lower than the uncertainty caused by the parameters for GWF prediction.

Fig. 12 displays the uncertainty of the models caused by the

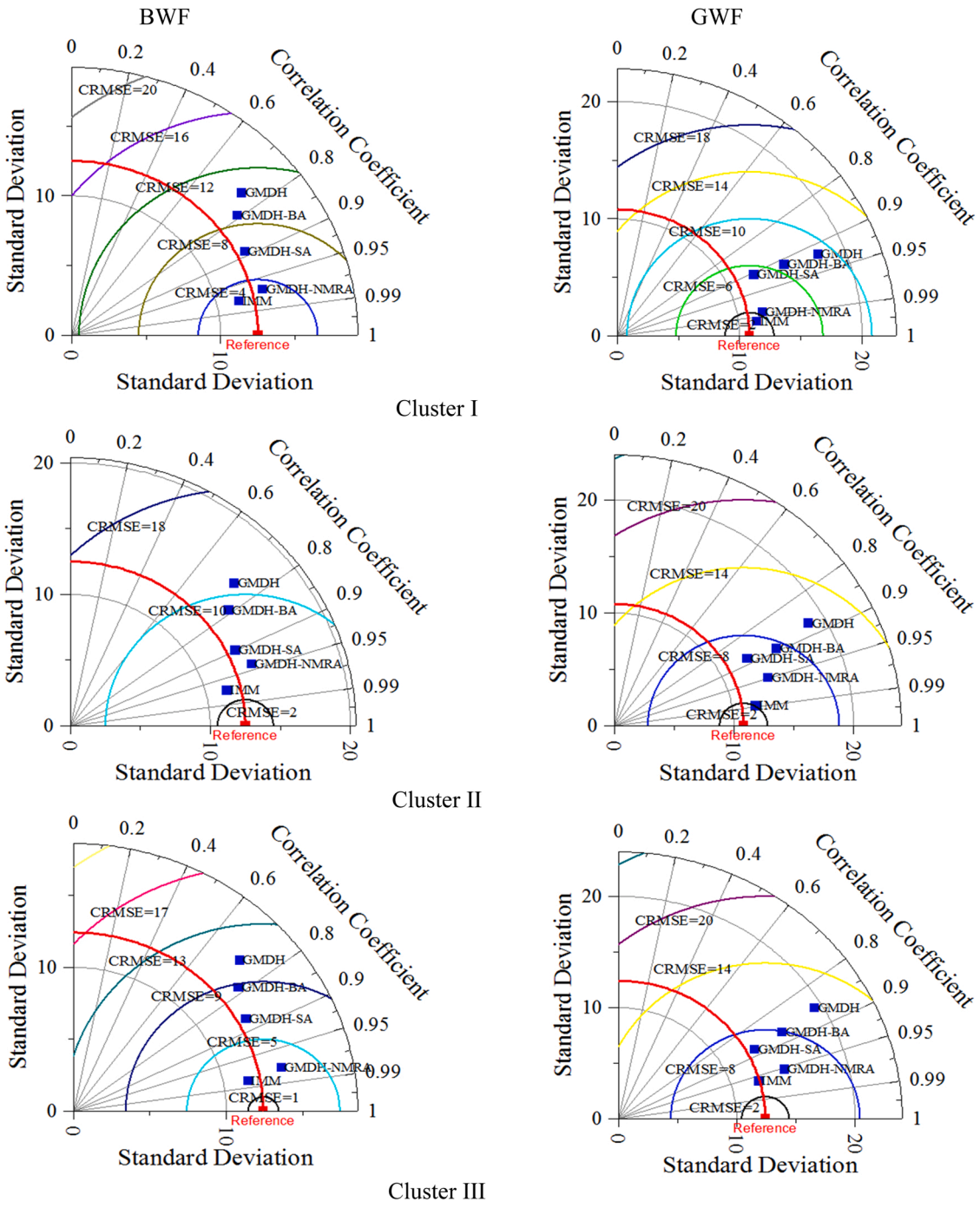

Fig. 14. Comparing models in predicting saffron BWF (left) and GWF (right) based on the Taylor diagram.

parameters and inputs. According to the results, the IMM and the GMDH NMRA models have the lowest (p = 0.98, r = 0.08) and the second lowest (p = 0.97, r = 0.09) uncertainties compared to the alternatives. Further investigation indicated that the uncertainty due to the inputs is lower than the parameters. The results also denoted that the optimization algorithms have been effective in reducing the uncertainty of the GMDH model given that the GMDH-hybrid models have lower uncertainty than the GMDH model.

4. Discussion

In this research, in order to measure the effect of inputs on the predicted values and determining the most effective predictors, the RMSE was used. This method has been widely used by researchers in agro-climatological and hydrological studies such as the sediment transfer rate modeling (Jalil-Masir et al., 2022), groundwater level prediction (Khozani et al., 2022) and daily pan evaporation (Ehteram et al., 2022a, 2022b). Therefore, regarding the number of input variables, 13 scenarios were considered such that in each, one input was eliminated and the influence was measured. Fig. 13 represents the effect of removing each predictor on the output of the GMDH NMR model.

As result shows, removing the ETC and yield, significantly increases the RMSE. Therefore, they are evaluated as the most effective inputs in predicting BWF and GWF. According to several studies (Papadavid and Toulios, 2018; Bazrafshan et al., 2019b) and FAO 33 or 56 or 66 equations (Allen et al., 1998), increasing (decreasing) evapotranspiration

directly affects the yield. On the other hand, the yield directly was included in GWF (in the denominator) Eq. (4). Therefore, removing these variables causes high sensitivity in model prediction. The error rate of removing individual variables is lower in GWF than in BWF. This indicates that the correlation between input variables in GWF is higher than in BWF.

Fig. 14 compares the performance of models based on the Taylor diagram. Taylor diagram is illustrated in two forms: half circle (denotes negative and positive correlation) and quarter circle (denotes positive correlation only). In both cases, the correlation coefficients are the radius of the circle on its arc, the standard deviations are the concentric circles with respect to the center and the RMSE values are drawn as concentric circles with respect to the reference point on the horizontal axis. The closer the location of the models to the reference point (black square on the horizontal axis), the better the model performance.

In order to evaluate the performance of IMM, the Taylor diagram was used. As shown for BWF in cluster I, the location of IMM is between the correlation coefficients 0.99 and 0.97 and the CRMSE is 2.5. In this regard, the best performance among various GMDH models belongs to GMDH NMRA, whose correlation coefficient is 0.97 and its CRMSE is 3. Results of Jalil-Masir et al. (2022) also indicates that the IMM performed better than the alternatives due to using the outputs of several optimized models.

Ensemble models combine several individual models which have several advantages (Abbaszadeh et al., 2021). the IMM is an ensemble model that applies the advantages of multiple individual models. Therefore, the IMM improves the performance of individual models with more flexibility (Ehteram et al., 2022a, 2022b).

The GMDH model with correlation coefficient 0.74 and CRMES= 9.93 has the worst performance in cluster I. The reason for the weak performance of GMDH is the training algorithm (gradient algorithm) and insufficient accuracy in finding the model parameters (Ehteram et al., 2022a, 2022b). Among GMDH models, the GMDH NMRA has the best performance in cluster I, with correlation coefficient 0.96 and CRMES= 3.0. The same results are obtained in clusters II and III.

According to Ehteram et al. (2022a, 2022b) in the NMR algorithm, worker and breeder balances the exploration and exploitation. Due to their large population size, workers perform exploration and breeders use more intensive exploitation than workers since they attempt to improve their compatibility in order to mate with queens. The NMRA algorithm can achieve better results when workers and breeders update themselves. Therefore, these algorithms produce better solutions such that low quality solutions are removed from optimization as breeders update themselves. Through the updating of NMR solutions, the problem space is investigated accurately.

The IMM also had better performance in predicting GWF than the alternatives. The noteworthy point is that all models have better performance in predicting GWF than predicting BWF. This issue was held in elimination the less effective variables in selecting best inputs which the main reason was the high correlation between input parameters in GWF compared to BWF.

Further analysis of Taylor diagram indicated that although the optimization algorithms increase the accuracy of GMDH, however the performance of models are different such that the GMDH-BA model has a weaker performance than the other GMDH hybrid models. This is due to the more ability of NMRA and SA than BA and PSO optimization algorithms in finding the absolute optimal answer for prediction models (Salgotra and Singh, 2019).

5. Conclusion

Increasing population, and consequently water demand in the agricultural sector and frequent drought events causes water resources management to be very important. Prediction water footprint is a key issue in the management of water resources and helps decision makers to have a true understanding of the volume of water consumed by the products. Therefore, prediction water footprints play a significant role in irrigation and agriculture management.

This study constructed a new ensemble model based on the improved GMDH models and investigated the model uncertainty due to the parameters and inputs and provided important step in predicting BWF and GWF indices.

Various climatic and crop inputs have been used to calculate the saffron BWF and GWF indices in major saffron production areas in Iran. In this regard, The FCM clustering method was used to determine the homogeneous agro-climatic of saffron cultivation areas in Khorasan region. Then, the most effective predictors in prediction BWF and GWF were selected using the step-by-step elimination and measuring their effect on GMDH NMRA output through 13 scenarios.

The GMDH model and various optimization algorithms such as NMRA, SA, BA, PSO, have been applied to predict the response variables. In the next step, the output of individual GMDH was included into the ensemble IMM model, and the uncertainty analysis of the model parameters and input was performed.

The present study indicated that applying the IMM and the optimized GMDH models improved the accuracy of the outputs. IMM performed better than the alternatives due to using the outputs of several individual models. Further analysis demonstrated that the uncertainty caused by the inputs was lower than the uncertainty caused by the model parameters.

Selecting the input variables is one of the important challenges in the present study. Another feature selection methods such as the gamma test, wavelet theory, principal component analysis and Boruta algorithm can be used to select the best input variables in the future studies. In this regard, collecting climatic and crop dataset was another limitation in modeling BWF and GWF indices. Although the IMM model may increase the accuracy, however collecting suitable dataset for training models is a complicated issue. The main finding of this research is that the ensemble models can improve the accuracy of optimized soft computing models. There are different ensemble models such as Bayesian model averaging (BMA) and copula Bayesian averaging model (CBMA). The advantage of IMM over BMA and CBMA is that the model does not have complex computations.

Although the optimization algorithms can enhance the performance of soft computing models, the optimized models are outperformed by the new ensemble models. This study indicated that the accuracy of models was affected by the uncertainty values. The model parameters and input parameters were the important uncertainty resources. The optimization algorithms can be used to set the model parameters. Thus, these algorithms can reduce the uncertainty values of models because of model parameters. The results of study also indicated that the optimization algorithms provided different accuracies because they used different and advanced operators. A robust optimization algorithm can decrease the uncertainty of model parameters.

The models introduced of the current study can be used for different regions of the world. These models can be coupled with climate scenarios to predict GWF and BWF under climate change. Thus, we can use the outputs of climate change models under different scenarios for predicting of GWF and BWF in the future periods.

Selecting best optimization algorithm is another issue of the present study. Choosing an optimization algorithm with fast convergence and high accuracy is very important, since a suitable optimization algorithm can reduce the model uncertainty caused by the parameters.

Measuring the model uncertainty caused by the parameters and inputs is another important result of the present study.

Applying the models of the present study is not limited to predicting BWF and GWF, but they could also be used to predict the other hydrological, hydroclimatic, drought and water resources variables. The results of the current research can also be extended in future studies to predict the BWF and GWF in various regions and products. Further, in future studies, the other ensemble models such as the Bayesian and

Bayesian copula can be used to improve the results. The next studies can use the methods such as gamma test and principal component analysis to choose the best inputs.

Declaration of Competing Interest

The authors declare that they have no known competing financial interests or personal relationships that could have appeared to influence the work reported in this paper.

Data availability

Will be sent upon request.

Acknowledgements

This research has been financially supported by the Saffron Institute, University of Torbat Heydarieh. The grant number was P/107266.

References

Abbaszadeh, M., Ehteram, M., Ahmed, A.N., Singh, V.P., Elshafie, A., 2021. The copper grade estimation of porphyry deposits using machine learning algorithms and Henry gas solubility optimization. Earth Sci. Inform. 14 (4), 2049–2075.
Abedinia, O., Amjady, N., Ghasemi, A., 2016. A new metaheuristic algorithm based on shark smell optimization. Complexity 21 (5), 97–116.
Adisa, J.A., Ojo, S.O., Owolawi, P.A., Pretorius, A.B., 2019, November. Financial distress prediction: principle component analysis and artificial neural networks. In: 2019 International Multidisciplinary Information Technology and Engineering Conference (IMITEC). IEEE, pp. 1–6.
Agayev, Y.M., Shakib, A.M., Soheilivand, S., Fathi, M., 2006. Breeding of saffron (Crocus sativus): possibilities and problems. In: II International Symposium on Saffron Biology and Technology 739, pp. 203–207.
Ahmed, B.T., Abdulhameed, O.Y., 2020. Fingerprint authentication using shark smell optimization algorithm. UHD J. Sci. Technol. https://doi.org/10.21928/uhdjst.v4n2y2020.pp28-39.
Al-Dyani, W.Z., Yahya, A.H., Ahmad, F.K., 2018. Challenges of event detection from social media streams. Int. J. Eng. Technol. (UAE). https://doi.org/10.14419/ijet.v7i2.15.11217.
Alizadeh, A., Sayari, N., Ahmadian, J., Mohammadian, A., 2009. Study for zoning the most appropriate time of irrigation of saffron (Crocus sativus) in Khorasan Razavi, north and southern provinces.
Allen, R.G., Pereira, L.S., Raes, D., Smith, M., 1998. Crop evapotranspiration-Guidelines for computing crop water requirements-FAO Irrigation and drainage paper 56 Fao, Rome, 300(9), D05109.
Bacanin, N., Arnaut, U., Zivkovic, M., Bezdan, T., Rashid, T.A., 2022. Energy efficient clustering in wireless sensor networks by opposition-based initialization bat algorithm. Lecture Notes on Data Engineering and Communications Technologies. https://doi.org/10.1007/978-981-16-3728-5_1.
Baghalian, K., Sheshtamand, M.S., Jamshidi, A.H., 2010. Genetic variation and heritability of agro-morphological and phytochemical traits in Iranian saffron (Crocus sativus L.) populations. Ind. Crops Prod. 31 (2), 401–406.
Bazrafshan, O., Gerkani Nezhad Moshizi, Z., 2019a. Assessment of water use efficiency and water footprint of saffron production in Iran. Saffron Agron. Technol. 7 (4), 505–519.
Bazrafshan, O., Etedali, H.R., Moshizi, Z.G.N., Shamili, M., 2019b. Virtual water trade and water footprint accounting of Saffron production in Iran. Agric. Water Manag. 213, 368–374.
Bhat, S.A., Pandit, B., Dar, M.U.D., Jan, R., Khan, S., Mehraj, K., 2017. Statistical comparison of reference evapotranspiration methods: a case study from Srinagar in J&K, India. Int. J. Curr. Microbiol. Appl. Sci. 6 (9), 3731–3737.
Cardone, L., Castronuovo, D., Perniola, M., Cicco, N., Candido, V., 2020. Saffron (Crocus sativus L.), the king of spices: an overview. Sci. Hortic. 272, 109560.
Chapagain, A.K., Hoekstra, A.Y., 2008. Globalization of water: sharing the planet's freshwater resources.
Constantinescu, R., White, J.T., Connor, C.B., Hopulele-Gligor, A., Charbonnier, S., Thouret, J. -C., Lindsay, J.M., Bertin, D., 2022. Uncertainty quantification of eruption source parameters estimated from Tephra Fall Deposits. Geophys. Res. Lett. https://doi.org/10.1029/2021gl097425.
Ehteram, M., Banadkooki, F.B., Fai, C.M., Moslemzadeh, M., Sapitang, M., Ahmed, A.N., Irwan, D., El-Shafie, A., 2021. Optimal operation of multi-reservoir systems for increasing power generation using a seagull optimization algorithm and heading policy. Energy Rep. https://doi.org/10.1016/j.egyr.2021.06.008.
Ehteram, M., Panahi, F., Ahmed, A.N., Mosavi, A.H., El-Shafie, A., 2022. Inclusive multiple model using hybrid artificial neural networks for predicting evaporation. Front. Environ. Sci. 9, 789995 https://doi.org/10.3389/fenvs.2021.789995.
Ehteram, M., Graf, R., Ahmed, A.N., El-Shafie, A., 2022. Improved prediction of daily pan evaporation using Bayesian Model Averaging and optimized Kernel Extreme Machine models in different climates. Stoch. Environ. Res. Risk Assess. 1–36.
Elbeltagi, A., Aslam, M.R., Malik, A., Mehdinejadiani, B., Srivastava, A., Bhatia, A.S., Deng, J., 2020a. The impact of climate changes on the water footprint of wheat and maize production in the Nile Delta, Egypt. Sci. Total Environ. 743, 140770.
Elbeltagi, A., Deng, J., Wang, K., Hong, Y., 2020b. Crop Water footprint estimation and modeling using an artificial neural network approach in the Nile Delta, Egypt. Agric. Water Manag. 235, 106080.
Elbeltagi, A., Azad, N., Arshad, A., Mohammed, S., Mokhtar, A., Pande, C., Deng, J., 2021. Applications of Gaussian process regression for predicting blue water footprint: case study in Ad Daqahliyah, Egypt. Agric. Water Manag. 255, 107052.
Ercin, A.E., Hoekstra, A.Y., 2016. European water footprint scenarios for 2050. Water 8 (6), 226.
Fallahi, H.R., Mahmoodi, S., 2018. Impact of water availability and fertilization management on saffron (Crocus sativus L.) biomass allocation. J. Hortic. Postharvest Res. 1 (2-September 2018), 131–146.
Hoekstra, A.Y., 2008. Water neutral: reducing and offsetting the impacts of water footprints. UNESCO-IHE Institute for Water Education.
Hoekstra, A.Y., Chapagain, A.K., 2006. Water footprints of nations: water use by people as a function of their consumption pattern. Integrated Assessment of Water Resources and Global Change. Springer, Dordrecht, pp. 35–48.
Hoekstra, A.Y., Hung, P.Q., 2003. Virtual water trade. In: Proceedings of the International Expert Meeting on Virtual Water Trade (vol. 12, pp. 1–244).
Hoekstra, A.Y., Chapagain, A.K., Aldaya, M.M., Mekonnen, M.M., 2011. The Water Footprint Assessment Manual: Setting the Global Standard. Routledge.
IRIMO, 2021. Iran Meteorological Bulletin. Islamic Republic of Iran Meteorological Organization Press, Tehran.
Ivakhnenko, A.G., 1968. The group method of data of handling; a rival of the method of stochastic approximation. Sov. Autom. Control 13, 43–55.
Ivakhnenko, A.G., 1971. Polynomial theory of complex systems. IEEE Trans. Syst. Man Cybern. 4, 364–378.
Jalil-Masir, H., Fattahi, R., Ghanbari-Adivi, E., Asadi Aghbolaghi, M., Ehteram, M., Ahmed, A.N., El-Shafie, A., 2022. An inclusive multiple model for predicting total sediment transport rate in the presence of coastal vegetation cover based on optimized kernel extreme learning models. Environ. Sci. Pollut. Res. 1–34.
Jamshidi, S., Imani, S., Delavar, M., 2020. Impact assessment of best management practices (BMPs) on the water footprint of agricultural productions. Int. J. Environ. Res. 14 (6), 641–652.
Kafi, M., Koocheki, A., Rashed, M.H. (Eds.), 2006. Saffron (Crocus sativus): Production and Processing. Science Publishers.
Kashani, A.R., Chiong, R., Mirjalili, S., Gandomi, A.H., 2021. Particle swarm optimization variants for solving geotechnical problems: review and comparative analysis. Arch. Comput. Methods Eng. 28 (3), 1871–1927.
Keykhamoghadam, P., Haghighi, Kamgar, Sepaskhah, A., Zand Parsa, A., S, 2013. Determination of single and dual crop coefficients and potential evapotranspiration of developed saffron. J. Agric. Meteorol. 1 (1), 1–13.
Khatibi, R., Nadiri, A.A., 2021. Inclusive Multiple Models (IMM) for predicting groundwater levels and treating heterogeneity. Geosci. Front. https://doi.org/10.1016/j.gsf.2020.07.011.
Khozani, Z.S., Banadkooki, F.B., Ehteram, M., Ahmed, A.N., El-Shafie, A., 2022. Combining autoregressive integrated moving average with Long Short-Term Memory neural network and optimisation algorithms for predicting ground water level. J. Clean. Prod. 348, 131224.
Kobarfard, M., Fazloula, R., Zarghami, M., Akbarpour, A., 2022. Evaluating the uncertainty of urban flood model using glue approach. Urban Water J. https://doi.org/10.1080/1573062x.2022.2053865.
Leone, S., Recinella, L., Chiavaroli, A., Orlando, G., Ferrante, C., Leporini, L., Menghini, L., 2018. Phytotherapic use of the Crocus sativus L.(Saffron) and its potential applications: a brief overview. Phytother. Res. 32 (12), 2364–2375.
Lu, S., Wang, S.H., Zhang, Y.D., 2021. Detection of abnormal brain in MRI via improved AlexNet and ELM optimized by chaotic bat algorithm. Neural Comput. Appl. https://doi.org/10.1007/s00521-020-05082-4.
Maghrebi, M.F., Vatanchi, S.M., 2021. Uncertainty analysis of stage-discharge curves by Generalized Likelihood Uncertainty Estimation (GLUE) method. Environ. Model. Assess. 26 (4), 447–458.
Mahdavi-Meymand, A., Zounemat-Kermani, M., 2020. A new integrated model of the group method of data handling and the firefly algorithm (GMDH-FA): application to aeration modelling on spillways. Artif. Intell. Rev. 53 (4), 2549–2569.
McCuen, R.H., Knight, Z., Cutter, A.G., 2006. Evaluation of the Nash–Sutcliffe efficiency index. J. Hydrol. Eng. 11 (6), 597–602.
Mekonnen, M.M., Hoekstra, A.Y., 2011. The green, blue and grey water footprint of crops and derived crop products. Hydrol. Earth Syst. Sci. 15 (5), 1577–1600.
Mekonnen, M.M., Hoekstra, A.Y., 2014. Water footprint benchmarks for crop production: a first global assessment. Ecol. Indic. 46, 214–223.
Ministry of Agriculture- Jihad (MAJ), 2021 (https://maj.ir/).
Mokhtar, A., Jalali, M., He, H., Al-Ansari, N., Elbeltagi, A., Alsafadi, K., Rodrigo-Comino, J., 2021. Estimation of SPEI meteorological drought using machine learning algorithms. IEEE Access 9, 65503–65523.
Mollafilabi, A., Davari, K., Dehaghi, M.A., 2020. Saffron yield and quality as influenced by different irrigation methods. Sci. Agric. 78.
Mugemanyi, S., Qu, Z., Rugema, F.X., Dong, Y., Bananeza, C., Wang, L., 2020. Optimal reactive power dispatch using chaotic Bat Algorithm. IEEE Access. https://doi.org/10.1109/ACCESS.2020.2982988.
Muller, J.A., Ivakhnenko, A.G., 1996. Self-organizing modelling in analysis and prediction of stock market. In Proceedings of the Second International Conference on Application of Fuzzy Systems and Soft Computing-ICAFS (vol. 96, pp. 491–500).
Muronda, M.T., Marofi, S., Nozari, H., Babamiri, O., 2021. Uncertainty analysis of reservoir operation based on stochastic optimization approach using the generalized

likelihood uncertainty estimation method. Water Resour. Manag. https://doi.org/10.1007/s11269-021-02877-5.
Papadavid, G., Toulios, L., 2018. The use of earth observation methods for estimating regional crop evapotranspiration and yield for water footprint accounting. J. Agric. Sci. 156 (5), 599–617.
Rahimi, J., Ebrahimpour, M., Khalili, A., 2013. Spatial changes of extended De Martonne climatic zones affected by climate change in Iran. Theor. Appl. Climatol. 112 (3), 409–418.
Rastegaripour, F., Mohammadi, N., 2018. Investigating Factors Affecting Currency Saffron in Iran with Emphasis on Packaging and Branding. (in Persian).
Rezaei, M., Mousavi, S.F., Moridi, A., Eshaghi Gordji, M., Karami, H., 2021. A new hybrid framework based on integration of optimization algorithms and numerical method for estimating monthly groundwater level. Arab. J. Geosci. https://doi.org/10.1007/s12517-021-07349-z.
Rosegrant, M.W., Ringler, C., Zhu, T., 2009. Water for agriculture: maintaining food security under growing scarcity. Annu. Rev. Environ. Resour. 34, 205–222.
Ruspini, E.H., 1969. A new approach to clustering. Inf. Control 15 (1), 22–32.
Salgotra, R., Singh, U., 2019. The naked mole-rat algorithm. Neural Comput. Appl. 31 (12), 8837–8857.
Seifi, A., Ehteram, M., Soroush, F., 2020. Uncertainties of instantaneous influent flow predictions by intelligence models hybridized with multi-objective shark smell optimization algorithm. J. Hydrol. https://doi.org/10.1016/j.jhydrol.2020.124977.
Shabani, E., Hayati, B., Pishbahar, E., Ghorbani, M.A., Ghahremanzadeh, M., 2021. A novel approach to predict CO_2 emission in the agriculture sector of Iran based on Inclusive Multiple Model. J. Clean. Prod. https://doi.org/10.1016/j.jclepro.2020.123708.
Shahidi, A., Behdani, M., Hjiabadi, F., Shirzadi, F., 2020. Determination of single and dual crop coefficients of saffron (Crocus sativus L.) in the first year of cultivation. J. Saffron Res. 4, 1–15.
Shourian, M., Jamshidi, J., 2022. Hedging rule-based optimized reservoir operation using metaheuristic algorithms. E3S Web Conf. 346, 02011 (EDP Sciences).
Siam, M.S., Eltahir, E.A., 2017. Climate change enhances interannual variability of the Nile river flow. Nat. Clim. Change 7 (5), 350–354.
Siddique, H.R., Fatma, H., Khan, M.A., 2020. Medicinal properties of saffron with special reference to cancer—a review of preclinical studies. Saffron 233–244.
Sidhu, B.S., Sharda, R., Singh, S., 2021. An assessment of water footprint for irrigated rice in punjab. J. Agrometeorol. 23 (1), 21–29.
Wang, F., Zhang, H., Zhou, A., 2021. A particle swarm optimization algorithm for mixed-variable optimization problems. Swarm Evolut. Comput. 60, 100808.
Wang, L., Li, L., Xie, J., Luo, Z., Sumera, A., Zechariah, E., Chen, Y., 2022a. Does plastic mulching reduce water footprint in field crops in China? A meta-analysis. Agric. Water Manag. 260, 107293.
Wang, X., Jia, R., Zhao, J., Yang, Y., Zang, H., Zeng, Z., Olesen, J.E., 2022b. Quantifying water footprint of winter wheat–summer maize cropping system under manure application and limited irrigation: an integrated approach. Resour. Conserv. Recycl. 183, 106375.
Wang, Y., Wang, P., Zhang, J., Cui, Z., Cai, X., Zhang, W., Chen, J., 2019. A novel bat algorithm with multiple strategies coupling for numerical optimization. Mathematics. https://doi.org/10.3390/math7020135.
Zhai, Y., Shen, X., Quan, T., Ma, X., Zhang, R., Ji, C., Hong, J., 2019. Impact-oriented water footprint assessment of wheat production in China. Sci. Total Environ. 689, 90–98.
Zhang, L., Liang, Y.Z., Jiang, J.H., Yu, R.Q., Fang, K.T., 1998. Uniform design applied to nonlinear multivariate calibration by ANN. Anal. Chim. Acta 370 (1), 65–77.
Zhang, Y., Huang, K., Yu, Y., Yang, B., 2017. Mapping of water footprint research: a bibliometric analysis during 2006–2015. J. Clean. Prod. 149, 70–79.
Zhang, Y., Huang, K., Yu, Y., Wu, L., 2020. An uncertainty-based multivariate statistical approach to predict crop water footprint under climate change: a case study of Lake Dianchi Basin, China. Nat. Hazards 104 (1), 91–110.
Zhao, X., Liao, X., Chen, B., Tillotson, M.R., Guo, W., Li, Y., 2019. Accounting global grey water footprint from both consumption and production perspectives. J. Clean. Prod. 225, 963–971.
Zhou, Y., Ye, J., Du, Y., Sheykhahmad, F.R., 2020. New improved optimized method for medical image enhancement based on modified shark smell optimization algorithm. Sens. Imaging. https://doi.org/10.1007/s11220-020-00283-6.
Zuo, D., Kan, G., Sun, H., Zhang, H., Liang, K., 2021. Improving computational efficiency of GLUE method for hydrological model uncertainty and parameter estimation using CPU-GPU hybrid high performance computer cluster. Nat. Hazards Earth Syst. Sci. Discuss. 1–33.